Spectroscopic methods for the study of artificial photosynthesis

Pieter Robaeys

promotor :
Prof. dr. Jean MANCA

co-promotor :
dr. Ludwig GORIS

Chapter 1

Acknowledgement

Icarus, I want to warn you to steer the middle course. This I want you to do, to prevent you to fly to low, where the waves of the sea will make the feathers in your wings heavier. But on the other hand, when you fly to high, the fires of the heaven will burn them. Just steer the middle road, and I command you not to look to Bootes, Helice or the pulled sword of Orion: just follow the journey under my guidance.

From the Greek legend of Daedalus and Icarus.

Like a lot of things in nature, everything exists in a fragile balance. Without it, the world would have a totally different aura then that we see in our surroundings every day. Also in order to complete this work, a balance was needed between sheer hard work and more relaxing times. Therefore, I've to thank a lot of people, for helping me keeping this balance.

First of all, I want to thank my promoter Prof. Dr. J. Manca and the Institute of Material Research (IMO), for giving me the opportunity to start with this thesis, and for the means for finishing it. I want to thank Dr. K. Vandewal, for the first immersion in the area of organic solar cells, and Dr. L. Goris for the further help as a supervisor and co promoter.

I also want to thank all the professors and assistants of Hasselt University for opening different windows for looking at the world we live in from different perspectives.

To balance the stress of working, I want to thank my co-leaders and the members of the Scouting group of Genk Centrum, for the wonderful Sunday afternoons I had. I also want to thank my fellow-students, at IMO, for the good laughs we had during dinner and for all the kinds of trivia we discussed.

Last but not least, I want to thank my family for standing by my side and supported me during good and bad times during my thesis and all the years before it.

Chapter 2

Abstract

The insatiable hunger for energy drives Western society to the limits of consumption of classical energy sources like fossil fuels. Undesired side effects of the use of these fuels are starting to rule over its benefits. The search for alternative energy harvesting techniques is of the greatest interest to find sustainable ways to support our way of living today. One of these branches of this extensive research domain is the research in organic solar cells. Until now a maximal efficiency with organic solar cells of 8% is reached. In order to improve these solar cells, a fundamental understanding of the working principle and its limits is necessary. In this thesis, a combination of two polymers, PFB and F8BT, is used. This polymer combination was investigated using morphological (AFM), optical (UV-Vis and fluorescence spectroscopy) and electrical techniques (IV-characterization and photocurrent measurements). All these techniques are used in order to search for relations between morphology, light absorption and emission, and electrical properties of these cells in order to get a better understanding of their working principles. Annealing at temperatures above the glass transition temperature of F8BT has shown that the morphological and optical properties of this blend contributed to fundamental changes of the active layer of these cells. Also a sub bandgap absorption band has been observed using photocurrent measurements, relating to the composition and molecular interactions in these solar cells. Although, this is just the beginning, these results are a first step to a general way of understanding the working principles of all polymer, organic solar cells.

De onuitputtelijke honger naar energie heeft de Westerse beschaving gedreven naar de limieten van de consumptie van de klassieke energie bronnen, zoals fossiele brandstoffen. Ongewilde bijwerkingen van het gebruik van deze brandstoffen beginnen door te wegen ten opzichte van de voordelen ervan. De zoektocht naar alternatieve manieren om energie te oogsten zijn dus van grootst belang om ervoor te zorgen dat onze Westerse manier van leven op verantwoordelijke wijze onderhouden kan blijven. Een van de takken van dit onderzoeksdomein is het onderzoek naar organische zonnecellen. Het efficintie record van vandaag voor organische zonnecellen ligt rond 8%. Om deze efficintie te verhogen is het nodig om een fundamenteel begrip te krijgen over de werkingsprincipes en limieten ervan. In deze thesis is er een combinatie van twee polymeren gebruikt: PFB en F8BT. Combinaties van deze twee polymeren werden bestudeerd met morfologische (AFM), optische (UV-Vis en fluorescentie

spectroscopie). Na het integreren van deze lagen in zonnecellen, elektrische technieken zoals stroom-spanning karakterisatie en fotostroom metingen werden gebruikt voor het onderzoeken van de foto elektrische eigenschappen van deze materialen. Een thermale behandeling van deze materialen bij temperaturen juist boven de glas transitie temperatuur van F8BT induceerde morfologische en optische veranderingen in deze polymeren. Door gebruik te maken van foto-elektrische metingen is er ook een sub-bandgap absorptie band waargenomen, welke gerelateerd kan worden aan de moleculaire samenstelling van deze cellen. Ondanks dat dit enkel het begin is, hebben deze resultaten een eerste stap gezet tot een algemeen beeld van de werkingsprincipes van alle organische zonnecellen.

Contents

Chapter 3

List of abbreviations

- AFM: Atomic force spectroscopy

- AM: Air mass

- AUC: Area under the curve

- CB: Conduction band

- CT: Charge transfer

- D/A: Donor acceptor

- DOS: Density of states

- DSSC: Dye sensitized solar cell

- E_g: Effective bandgap energy

- EQE: External quantum efficiency

- F8BT: Poly(9,9-dioctylfluorene-co-benzothiadiazole)

- FF: Fill factor

- FTIR: Fourier transform infrared spectroscopy

- FTO: Fluorine tin oxide

- FTPS: Fourier transform photocurrent spectroscopy

- HOMO: Highest occupied molecular orbital

- IMO: Instituut voor materiaal onderzoek

- I_{max} Current at maximal power

- IR: Infra red

- I_{sc}: Short circuit current

- ITO: Indium tin oxide

- IV: Current voltage

- LHE: Light harvesting efficiency

- LUMO: Lowest unoccupied molecular orbital

- MDMO:PPV: poly[2-methoxy-5-(3,7-dimethyloctyloxy)-1,4-phenylene-vinylene]

- MilliQ: demineralized

- P3HT: poly(3-hexylthiophene)

- PC: photocurrent

- PCBM: phenyl-C61-butyric acid methyl ester

- PEDOT:PSS: Poly(3,4- ethylenedioxythiophene)-polystyrene sulfonate

- PFB: Poly(9,9-dioctylfluorene-co-bis-N,N-(4-butylphenyl)-bys-N,N-phenyl-1,4-phenylenediamine)

- RMS: Root mean square

- T_g: Glass temperature

- UV: Ultra Violet

- VB: Valence Band

- Vis: Visual

- V_{max}: Voltage at maximal power

- V_{oc}: Open circuit voltage

Chapter 4

Introduction

4.1 Conductive polymers: a surprising discovery

Advanced conjugated polymers are nowadays attracting considerable interest with regard to their numerous applications in microelectronics [1], nonlinear optics [2], magnetism [3] and specific interactions with inorganic species [4]. Such polymers are commonly used in practical applications such as polymer light-emitting diodes [5], organic field-effect transistors [6], anti static layers [7], solar cells [8] and sensors [9]. In 2000 Alan J. Heeger, Alan G. MacDiarmid, Hideki Shirakawa [10]were awarded the Nobel Prize in Chemistry for their extensive research in the field of conjugated polymers.

A key property of a conductive polymer is the presence of conjugated double bonds along the backbone of the polymer. In conjugation, the bonds between the carbon atoms are alternately single and double. Every bond contains strong localized 'sigma' (σ) bonds. In addition, every double bond contains a delocalized 'pi' (π) bond. However, conjugation is not enough to make the polymer material conductive. Charge carriers in the form of extra electrons or holes have to be injected into the material [10]. This can be achieved by chemically doping the materials in order to vary the conductivity such that a range from insulating, over semi-conducting to metallic properties are feasible.

An overview of the conductivity of materials can be seen in figure 4.1
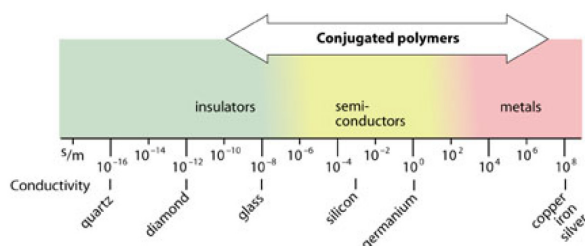
Figure 4.1: Conductivity of conjugated polymers compared to those of other materials, from quartz (insulator) to copper (conductor)[10].

In 1872, Ludwig Boltzmann described the thermal properties of electrons in a system. He

described that the fractional number of electrons $\frac{N_i}{N}$ occupying a set of states i and possessing an energy E_i as [11] [12]:

$$\frac{N_i}{N} = exp(-\frac{E_i}{k_B T}) \tag{4.1}$$

Where T is equal to the temperature of the system and k_B is Boltzmann's constant.

The electronic properties of materials can also be described by quantum mechanics [10] [12][13]. Here it is assumed that all materials consist of atoms, and/or combinations of atoms (molecules). The atom itself is made up by positive protons and neutral neutrons present which form nucleus. Around this nucleus a cloud of negatively charged electrons are present to preserve the charge neutrality of the atom. These electrons can be considered as free particles in a box. The energy is given by the following equation:

$$E_n = \frac{n^2 h^2}{8m(Nd)^2} \tag{4.2}$$

Where h is the Planck's constant, N the number of electrons separated by a distance d. m is the mass of the electron and n is a referred to as the quantum number. So the energy of an electron can be considered as quantified by the quantum number n. This is in contrast to the description by Boltzmann, where the energy distribution of an electron is continuous. In addition, the electrons are present in pairs with different electron spins. This is necessary according Pauli's exclusion principle where all the electrons in a system have a unique set of quantum numbers.

In the case of a semiconductor, electrons present in the highest occupied molecular orbital (HOMO) is given by:

$$E_{HOMO} = \frac{(\frac{N}{2})^2 h^2}{8m(Nd)^2} \tag{4.3}$$

The energy of the lowest unoccupied molecular orbital (LUMO) is given by

$$E_{LUMO} = \frac{(\frac{N}{2} + 1)^2 h^2}{8m(Nd)^2} \tag{4.4}$$

When the electrons are driven to cross the gap from the HOMO to the LUMO of a material, they have to bridge an energy gap, given by:

$$\Delta E = E_{LUMO} - E_{HOMO} \tag{4.5}$$

This energy gap is also known as the bandgap of the material. If this gap is very small, electrons in the valence band (VB) can gain thermal energy to cross over to the conduction band (CB) and take part in the conduction process. This gives the intrinsic conductivity of the semiconductor.

The distribution of electrons over energy is described by the Fermi-Dirac distribution published by E. Fermi and P. Dirac in 1926. At a temperature of 0K, it is 100% certain that all the electrons are present in energy states smaller or equal to E_f. The probability that the energy state E is occupied by an electron is given by f(E):

$$\begin{aligned} E < E_f &\rightarrow f(E) = 1 \\ E > E_f &\rightarrow f(E) = 0 \end{aligned} \tag{4.6}$$

When $T > 0$, some of the electrons will have enough energy to be excited, and to jump from the HOMO-state to the LUMO-state leaving a vacant energy level behind. This will happen only for the electrons with energies close to E_f, because electrons with lesser energy have less chance to get an energy boost large enough to free them from their previous position. Fermi and Dirac combined the classical description of the temperature-dependent behaviour of an electron described by Boltzmann with the quantum mechanical description of the energy of electrons into a new theory based on the Fermi-Dirac distribution. This relation is given by:

$$f_e(E) = \frac{1}{1 + exp(\frac{E - E_F}{kT})} \tag{4.7}$$

Here $exp(\frac{E - E_f}{kT})$ represents the Boltzmann energy distribution of electrons at temperature T. The change of occupation at different temperatures is illustrated in figure 4.2 a.

When the electron leaves the HOMO of the material, a hole stays behind. The occupation of holes is given by $1 - f_e(E)$ and is equal to:

$$f_h(E) = 1 - f_e(E) = 1 - \frac{1}{1 + exp(\frac{E - E_F}{kT})} \tag{4.8}$$

This relationship is illustrated in figure 4.2 b.
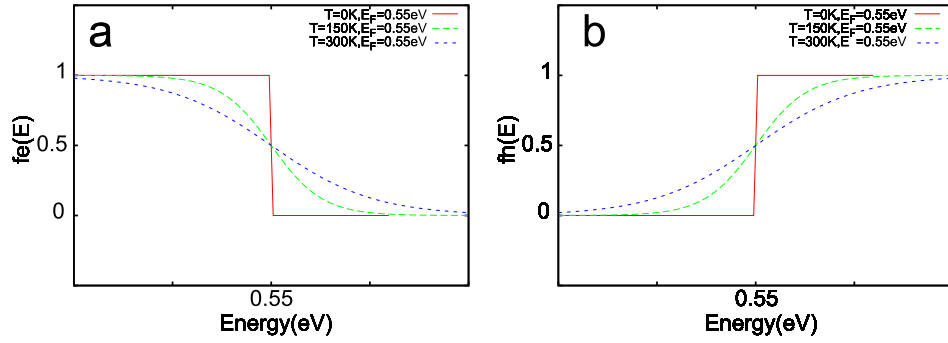
Figure 4.2: (a) The Fermi-Dirac distribution $f_e(E)$, describes the probability of finding a set of electrons with an energy E=0.55eV in the state below the Fermi energy. (b) The Fermi-Dirac distribution $f_h(E)$, describes the probability of finding a set of holes state below the Fermi energy. This is both done at a temperature of 0K, 150K and 300K.

E_f is by definition the energy at which the probability to obtain the occupation of the level equal to $\frac{1}{2}$. The Fermi-Dirac equation can be multiplied with the *density of states*(DOS), in order to obtain the number of occupied states as a function of energy. The DOS describes the number of states at each energy level that are available to be occupied. A high DOS at a specific energy level means that there are many states available for occupation. A DOS of zero means that no states can be occupied at that energy level. So for semiconductors, the concentration $n_o(E)$ of occupied states in the conduction band at a certain energy E is given by [14]:

$$n_o(E) = D(E)f_e(E) = \frac{D(E)}{1 + \frac{exp(E - E_f)}{kT}} \tag{4.9}$$

The concentration n_u of unoccupied states per energy in the valence band is likewise

$$n_u(E) = D(E)f_h(E) = D(E) - \frac{D(E)}{1 + \frac{exp(E-E_f)}{kT}} \tag{4.10}$$

It has to be noted that the description focused on charge carriers in a semiconductor. In a more fundamental approach one uses the chemical potential μ of the particle in question instead of E_f.

4.2   Organic Solar Cells

For already a few billion of years, photosynthetic organisms have been thriving on the abundance of water and CO_2. Under high temperature and pressure and millions of years of time, the remains of these organisms convert into 'fossil fuels'. In 1712, Savery and Denis Papin began using these 'fossil fuels' as heat source for the production of steam in the first commercial steam engines, paving the road to the industrial revolution [15]. Since then, western society has thrived on the use of these fuels. Its fuel dependent population expanded as never before. The oil crisis in 1973 and the more recent crisis in the Middle East illustrate how fragile this dependency is. Besides human dependency on fossil fuels, its exploitation and use have enormous consequences on the environment we all depend on. The recent failure of the Deep water Horizon oil rig shows how balancing on the edge of technical abilities ended in an incomprehensible natural disaster in the Gulf of Mexico [16]. Moreover, during the industrial revolution, lots of fossil fuels were burned, leading to increased amounts of CO_2 in the atmosphere. Because CO_2 is a greenhouse gas, it tends to prevent solar energy from leaving the earth surface, contributing to a global warming effect. It is possible that the consequences of global warming will induce dramatic changes in the climate. Therefore, people started to search for energy alternatives, in water-, wind- and solar energy. The latter is a very promising form of energy because it can be harvested everywhere on the planet. And most important of all, it is plentiful: $3.10^{24} \frac{J}{year}$ reaches the Earth's surface, 10^4 times the amount equivalent to the energy needs of today's world population [17]. The only problem left now is how to harvest this energy efficiently?

One of approaches is the study of the process where it all started with: photosynthesis. The first approach to build an artificial variant on this process dates back from 1968 [18], where chlorophyll was used to sensitize a metal oxide. Later on, chlorophyll was replaced by more efficient ruthenium complexes [17]. The integration of this system in an electrochemical cell is referred in the field as dye sensitized solar cells (DSSC). The working principle of DSSC's is described as follows: when light reaches the reactive metal core of the pigment molecule, its electrons are excited and are released in the CB of the metal oxide. This will lead to charge separation of electrons and holes. The free electron will travel through the metal oxide layer till an ITO or FTO layer is reached. This layer is connected to an external circuit. After running through this external circuit the electron reaches a metal back electrode. Here it will be taken up by an iodide/triiodide redox-electrolyte that will function as an electron carrier, which will return the electron to the metallic core of the dye complex. Now the process can start all over again. The efficiency of these cells are around 11% nowadays [19].

During the 1980's, all organic pn-junctions consisting of of donor and acceptor materials were introduced (figure 4.3 (a)). These cells consist of a layered electron donating (donor) and electron accepting (acceptor) organic molecules or polymers. When light with sufficient

energy shines on these cells electrons in the donor layer are excited forming electron hole pairs or excitons. These pairs have a large binding energy. So the electrons have not enough energy to split efficiently from their holes. Instead, these excitons diffuse through the donor layer to reach the interface with the acceptor where electron transfer will occur from donor to acceptor. Since the diffusion length of these excitons is only 10 nm, (this region is also called the photo-active region), only these excitons will diffuse to the interface and will form free charges. After efficient splitting of these excitons the electron is conducted through the acceptor layer to the anode. The hole on the other hand will travel through the donor layer to the cathode. After the transport of the electron through the electrical circuit, it will reach the cathode where it will recombine with the hole. A big disadvantage of these devices is that a relatively large part of the excitons cannot reach the donor acceptor (D/A) -interface, because the distance they have to travel to the D/A-interface was bigger than the diffusion length of this exciton (around 10 nm). So large parts of these pairs recombine without creating free electrons.

This is why in the 1990's bulk heterojunctions were introduced (figure 4.3 (b)). The working principle of these cells is comparable with that of a bilayered organic solar cell. The only difference is that the active layer is a blend of the donor and acceptor material in order to reduce the distance that the excitons have to travel to the interface, to the diffusion length of 10nm. So the amount of excitons, efficiently separated in charges, present in the photo-active region rises a lot compared to the double layer setup. In this way, the charge generating area is largely extended since in this diffuse interlayer excitons are always in close proximity to the charge separating D/A interface.
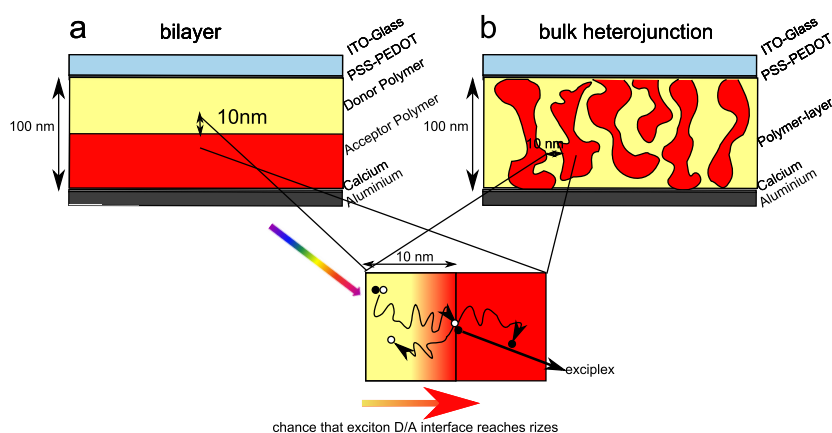
Figure 4.3: Schematic illustration of a polymer-bilayer solar cell(a) and a polymer-bulk heterojunction solar cell (b). In both cases an active layer of 100 nm thick is present sandwiched between a poly(3,4- ethylenedioxythiophene)-polystyrene sulfonate (PEDOT:PSS) layer connected to the ITO-electrode. On the other side the active layer is connected with a metal counter electrode.

High efficiencies of $5-6\%$ have been achieved with these bulk heterojunction solar cells. In previous times, the electron donor poly[2-methoxy-5-(3,7-dimethyloctyloxy)-1,4-phenylene-vinylene] (MDMO-PPV) was used in combination with a lot of different electron-acceptors, reaching efficiencies of 3% [8]. Later, regioregular poly(3-hexylthiophene)(P3HT): phenyl-

C61-butyric acid methyl ester(PCBM) replaced MDMO-PPV:PCBM as dominant absorber layer in solar cells, reaching efficiencies of 4% [8]. Recently, a company called Solarmer has set the record for organic solar cells at an efficiency of 8% [20].

4.3 Solar Energy

4.3.1 Solar Power

As described in [21], the sun radiates energy as if it were a black body, described by Planck, with a surface temperature of 5762 K. Before this light reaches the earth it has to travel a distance of $r_{s-e} = 1,5.10^{11}m$. The average power of the sun reaching the outer Earth atmosphere is equal to $1366.1\frac{W}{m^2}$. Before this energy reaches the Earth surface, the light has to travel through the atmosphere.

This atmosphere modifies the solar spectrum reaching the Earth surface [22], absorbing a lot of infrared (IR) and ultraviolet (UV) light from the Sun, depending on the latitude at which one would measure its spectrum.

Because of these differences, international standard solar spectra have been determined. Three standards can be used: the Air Mass (AM)0, AM1 and AM1.5 global (g). An overview of these spectra is illustrated in figure 4.4. Before entering the atmosphere, the light spectrum is called AM0 (black curve in figure 4.4) . At the surface on the equator, the light spectrum is termed AM1 (red curve in figure 4.4). The AM1.5g is used for the spectrum that is received all over the globe on places where the sunlight travels 1.5 times the distance through the atmosphere compared to the distance it has to travel at the equator (green curve in figure 4.4). For this thesis a solar simulator emitting light with a power of $1000\frac{W}{m^2}$ has been used. This is according to the AM1.5g spectrum.
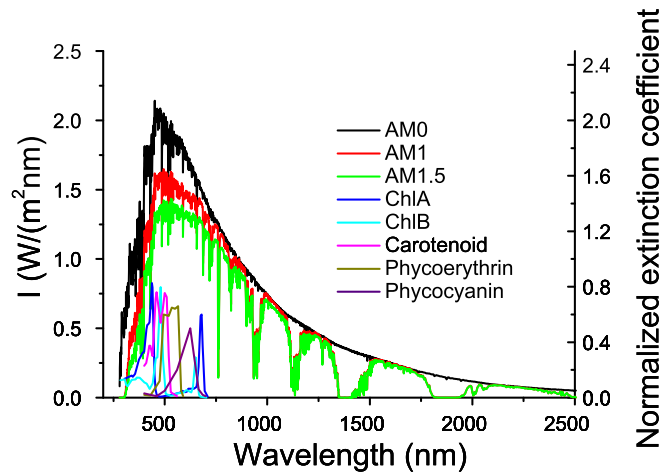
Figure 4.4: The spectral radiance measured outside the Earth's atmosphere AM0, on the Earth surface near the equator AM1, on the Earth surface in the northern hemisphere (AM1.5)[21]. Also measured in vivo absorption spectra of photosynthetic pigments of plants and algae are presented [23].

In figure 4.4, the absorption spectra of some very common pigments that are used by living organisms to convert light with usable energy are also displayed. It is obvious that these spectra overlap with the high intensity of the solar irradiation.

4.3.2 Optical properties of semiconductors: Absorption and emission rates and the importance of the interface

When light interacts with matter, a delicate equilibrium exists between light absorption and emission according to the absorption and emission rate. In 1917 Einstein described this phenomenon for atoms in his study 'On the quantum theory of radiation' [24]. From this relation, Strickler and Berg derived a variant for molecules (1962) [25].

This relation between absorption and emission is quite important to understand the photon-electron interactions in solar cells. It implies that molecules with a high absorption rate, will also have a high emission rate. This will unavoidably lead to a lower lifetime of the excited state. A good working solar cell needs a high absorption rate. But for the excited molecule to dissociate into free carriers, which are then transported to the electrodes, a low emission rate is necessary. So, the understanding of the delicate balance between these two rates is important to improve the efficiency of solar cells.

The relation between the absorption and emission intensity and the Einstein coefficients A and B are given in the Strickler- Berg derivation. Here it has been shown that for the absorption rate the relation is given by [25]:

$$B_{ground \to excited} = \frac{2303}{hnR_A} \int \varepsilon dv \qquad (4.11)$$

The emission rate is given by

$$A_{excited \to ground} = \frac{8 * 2303\pi n^2}{c^2 R_A} \frac{\int I(v)dv}{\int v^{-3} I(v)dv} \int \varepsilon dv \qquad (4.12)$$

For the derivation of these formula, the energy of the light is expressed in frequency v ($\frac{1}{s}$). For the absorption rate, the extinction coefficients are integrated over all energies. R_A is Avogadro's number. The refractive index of the surface is n and h is Planck's constant. The speed of light in a vacuum is given by c. For the emission rate, the fluorescence intensities are integrated over all frequencies.

Not only the absorption and emission properties of the pure materials are important. Since in organic solar cells the junction is of a molecular nature, the interaction properties between them are of major importance. Due to the electronic interactions of donor and acceptor materials at the interface the local behaviour of the polymers will change, leading to the stabilization of the molecular complex. This stabilized complex is also known as the charge-transfer complex. In the course of this thesis, the presence of this complex is investigated for an all polymer solar cell consisting of poly(9,9-dioctylfluorene-co-bis-N,N-(4-butylphenyl)-bys-N,N-phenyl-1,4-phenylenediamine) (PFB) as donor material and poly(9,9-dioctylfluorene-co-benzothiadiazole) (F8BT) as acceptor. A schematic representation of this charge transfer interaction in these materials is shown in figure 4.5.
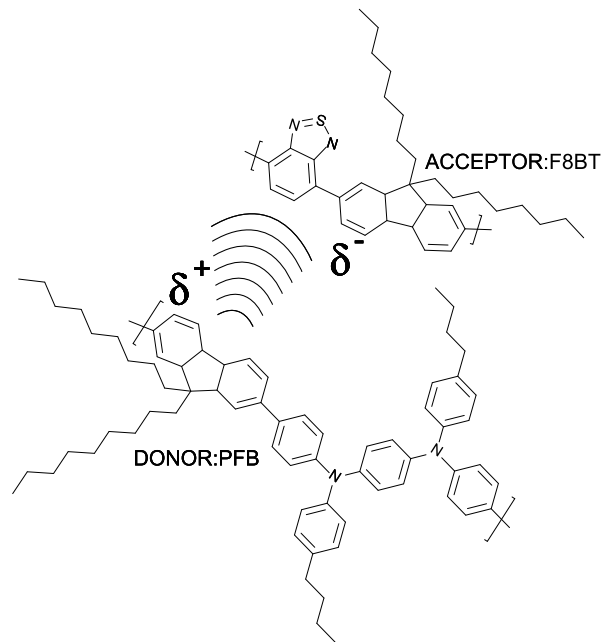
Figure 4.5: General view of a charge transfer complex between the donor (PFB) and acceptor (F8BT) materials used for this thesis.

The nature of the forces in a charge-transfer (CT) complex is not a stable chemical bond and is much weaker than covalent forces, it would rather be characterized as a weak electron resonance. As a result, the excitation energy of this resonance occurs very frequently in the visible- and IR-region of the electro-magnetic spectrum. These optical absorption bands are often referred to as CT-bands. Such interactions were formerly detected by the application of highly sensitive spectroscopic methods. This was done using blends consisting of organic donor materials in combination with PCBM [21]. In this thesis, the same techniques will be used to investigate this phenomenon in all polymer solar cells.

4.4 Efficiency of a solar cell

4.4.1 Power conversion efficiency

To determine the efficiency of a solar cell, the output current (I) is measured as a function of the applied voltage (V) as represented in a current voltage (IV) characteristic [26]. A typical IV-characteristic can be seen in figure 4.6 (a).
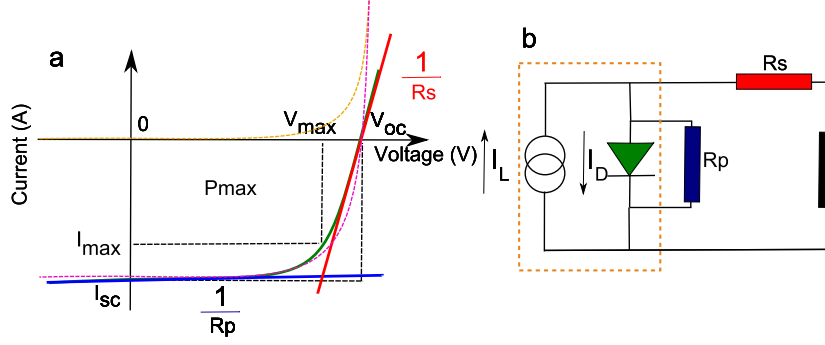
Figure 4.6: IV-curve of a solar cell. An ideal diode is represented in the orange dashed line. The IV-characteristic of a real solar cell is represented by the green line. (b) An equivalent scheme of a solar cell is described here.

If no light is applied on an ideal solar cell, the dark current (I_D) will follow the IV-characteristic of a diode (the orange dashed line in figure 4.6(a)) and can be expressed as [13]:

$$I_D = I_0(exp(\frac{qV}{kT}) - 1) \tag{4.13}$$

Here, I_0 is the reverse saturation current. During the illumination on this ideal solar cell, the position of I_0 will shift according to an opposing light current I_L as described in figure 4.6(b). In this situation, the IV-characteristic is represented by the purple curve in 4.6(a) and described by the equation below:

$$\begin{aligned} I &= I_D + I_L \\ &= I_0(exp(\frac{qV}{kT}) - 1) - I_L \end{aligned} \tag{4.14}$$

A real solar cell's behaviour deviates from ideal, represented by the purple curve in figure 4.6a. The IV-characteristics of real solar cells is described by the green line in figure4.6 and this is described by the equation below [27]:

$$I = I_L - I_0(exp(\frac{qV + R_sI}{kT}) - 1) - \frac{V + R_sI}{R_p} \tag{4.15}$$

Here, there are some important parameters:

- I_{sc} is the short circuit current. This is the equivalent for I_L.

- V_{oc} is the open circuit voltage. This is the voltage where the net current flowing is equal to 0A.

- The generated power by this solar cell is maximal at (P_{max}). This value is determined by I_{max} and V_{max}.

- R_s is a the resistance caused by impurities at the metal-polymer contacts [27].

- R_p is the resistance as a result of lost currents [27].

According to Ohm's law, the values of R_s and R_p can be calculated from the first derivate of the IV-characteristic. $\frac{1}{R_s}$ is the value of the first derivate of the JV-characteristic when $V = V_{oc}$. $\frac{1}{R_p}$ is the resistance when $V = 0V$. In the ideal case R_s is zero and $R_p = \infty$ [27].

When the IV-characteristic of the solar cell is known, it is possible to calculate the power of this cell by making the product between the current and the voltage at each point of the curve. The coordinate of the voltage and current where the power is maximal can be denoted as the maximal power point(V_{max},I_{max}). After determining V_{oc} and I_{sc} the fill factor FF can be easily determined by:

$$
\begin{aligned}
FF &= \frac{P_{max}}{I_{sc}V_{oc}} \\
&= \frac{I_{max}V_{max}}{I_{sc}V_{oc}}
\end{aligned}
\tag{4.16}
$$

This fill factor FF can thus be represented as the area of the IV-characteristic.

The efficiency η can be defined as the ratio of the maximal power of the solar cell and the power of the polychromatic light falling on it. It is given by [21]:

$$
\begin{aligned}
\eta &= \frac{P_{max}}{P_{light}} \\
&= \frac{I_{sc}V_{oc}FF}{P_{light}} \\
&= \frac{I_{max}V_{max}}{I_{sc}V_{oc}} \frac{I_{sc}V_{oc}}{P_{light}} \\
&= \frac{I_{max}V_{max}}{P_{light}}
\end{aligned}
\tag{4.17}
$$

4.4.2 Photon-to-electron conversion efficiencies

It is also very useful to determine the efficiency of which a photon with a certain energy will contribute to the photo-current. This efficiency is also called the external quantum efficiency (EQE) or incident photon to current conversion efficiency. This relation is given by the following equation:

$$
\begin{aligned}
EQE &= LHE(\lambda)\phi_{inj}\eta_{coll} \\
&= \frac{N_e^{out}}{N_{ph}^{in}}
\end{aligned}
\tag{4.18}
$$

The light harvesting efficiency (LHE) for photons at a wavelength λ is represented by $LHE(\lambda)$. This is equivalent to the absorption coefficient. ϕ_{inj} is defined as the quantum yield for electron injection from the excited donor into the LUMO of the acceptor and η_{coll} is the charge collection efficiency [17]. This equation can also be seen as the ratio of number of electrons leaving the system N_e^{out} and the number of photons with a wavelength λ falling on the device N_{ph}^{in} [21].

4.5 Used conjugated polymer combination: F8BT and PFB

4.5.1 Chemical structure and uses in organic solar cells

Polyfluorenes are photoelectric active materials which can be used over the whole visible range of the solar spectrum [28]. Provided that the maximum phase size is of the order of the exciton diffusion length, excitons can be split across heterojunctions with near unit efficiency, even with minimal band-edge offsets [29]. Quenching of fluorofores is caused by the prevention of irradiative relaxation of excited electrons [30]. This can be done by radicalization, where the excited electron is transferred from the electron donor to the acceptor. Another possibility is the transfer of the excitation energy from donor to acceptor, where the electron in the donor material relaxes but the emitted energy is directly transported to the acceptor, which will be excited.
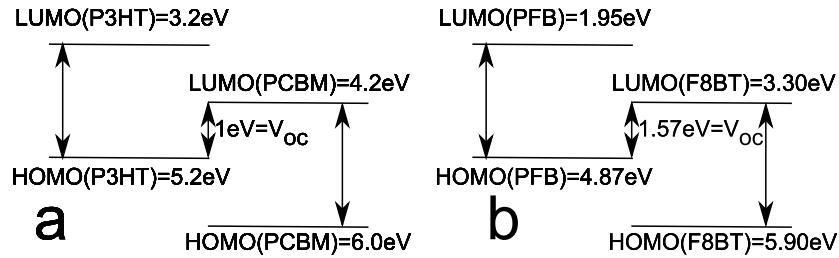
In this thesis we investigated the effect of annealing on the fluorescence and absorption properties as a function of the relative fraction of the donor PFB in the acceptor F8BT as can be seen in figure 4.7. Moreover the sub-bandgap absorption properties of these annealed films were measured by photocurrent spectroscopy.
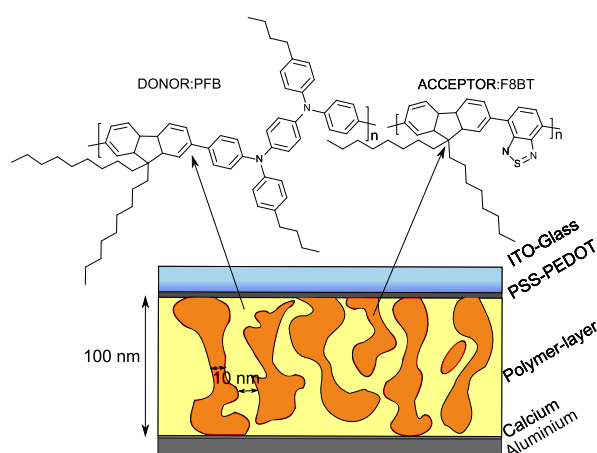
Figure 4.7: The polymer-polymer combination used in this thesis. PFB was used as a donor material while F8BT functioned as acceptor. Blends with different fractions of these two polymers were investigated here in function of fraction and annealing effects.

This D/A-system has been investigated by Friend et al. for the use in organic solar cells. PFB is a conjugated polymer that absorbs light at 426 nm. The maximal emission intensity can be seen at 450nm. F8BT has a maximal absorption intensity about 475nm, and emits at 540nm. These values can be correlated to cyclic voltometric measurements done by [30].

It has been seen in [21] that the charge transport over the junction is correlated with the presence of exciplexes in the photo-current spectra of different donor polymers in combination with PCBM as electron acceptors. This combination was relevant to study because the most efficient devices are made from polymer blends of donor molecules in combination with electron acceptors high electron affinities, such as fullerene derivatives. But in these blends, large band-edge offsets reduce the available open-circuit voltage and fundamentally limit the photo voltaic efficiency is shown in figure 4.8.

LUMO(P3HT)=3.2eV   LUMO(PFB)=1.95eV

LUMO(PCBM)=4.2eV   LUMO(F8BT)=3.30eV

1eV=V_{oc} 1.57eV=V_{oc}

HOMO(P3HT)=5.2eV   HOMO(PFB)=4.87eV

a   **b**

HOMO(PCBM)=6.0eV   HOMO(F8BT)=5.90eV

Figure 4.8: Band scheme of (a) a material combination of $P3HT : PCBM$ compared with (b) a $PFB : F8BT$ blend. It is indicated that V_{oc} for $PFB : F8BT$ blends is higher than for $P3HT : PCBM$.

In part (a) a representation is made between the HOMO-LUMO band schemes of a P3HT:PCBM combination which has an efficiency of approximately 3% and with a V_{oc} of around 1V. On the other hand, a HOMO-LUMO band scheme of a PFB:F8BT blend is represented in figure 4.8 b. It can be observed that the V_{oc} for this blend is around 1.57V. One should expect, that the efficiency should by higher due to the higher value of V_{oc}, but it is seen that the efficiency of these solar cells are a lot lower.

The reason that material combinations with low band-edge offsets have so far failed to outperform the solar cells made from fullerene derivatives, can be found in the transport and recombination mechanisms for the free charges in the bulk materials [30].

It has also been demonstrated that heating the active layer of the device to a temperature greater than the glass temperature T_g. This allows 1) the polymer chains to reorganize and 2) the acceptor molecules to freely diffuse into the composite and reorder in a more thermodynamically favorable way [31]. This reflected in higher hole mobilities, higher FFs and reduced serial resistances [8]. It has already been observed that controlled annealing of intimately mixed PFB:F8BT blends have impact on nanoscale phase separation. A distinct phase separation has been noticed for 140 and 160C annealed films with domain sizes of 18 ± 4 and 35 ± 8 nm, respectively, measured from cross sectional profiles. The evolution of morphology over this temperature range corresponds to a glass transition temperature of 140C for F8BT and PFB [29].

Besides these classical absorption and emission bands, also a characteristic exciplex emission can also be noticed at 630nm. Until now, the exciplexes in the PFB:F8BT blends were only studied with optical techniques (light emission) [30]. In this thesis thesis an attempt was made to reveal the existence of exciplex formation with high sensitive spectroscopic techniques such as Fourier transform photo-current spectroscopy and conventional photo-current spectroscopy [21] and [26].

Chapter 5

Material and Methods

5.1 Optical techniques

5.1.1 Sample preparation

Samples for optical measurements consist of a glass substrate with a spin coated layer ($\pm 100nm$) of the organic compound under investigation.

Glass substrates were cut from microscope slides (Thermo scientific) into spectrometer specific dimensions. They were mechanically cleaned with a honeycomb wiper permeated with a soap solution ($\frac{soap}{water} = \frac{1}{20}$) (BUEHLER ultramet 2 sonic cleaning solution). The substrates were ultrasonically cleaned for 30 minutes in the soap solution and rinsed with MiliQ-water. After the washing, the substrates were ultrasonically cleaned in acetone for 15 min, followed by boiling in isopropanol for 10 minutes. Acetone and isopropanol were obtained from VWR. After cleaning they were dried using a nitrogen flow.

Polymer mixtures were obtained by making solutions ($10\frac{mg}{ml}$) of PFB (MW: 80000-120000) (American Dye Source) and F8BT (MW: 5000-8000) (Sigma Aldrich) in chloroform (with 0.6% ethanol) (VWR) in a nitrogen environment. After stirring for 24 hours the pure materials were blended in fractions of 0.2-0.8 in steps of 0.1. These solutions were spincoated on the cleaned glass substrates at 700 rpm for 2 minutes. Layers with a thickness of around 100-150nm were obtained. These values were confirmed by the use of DEKTAK measurements.

Optical spectroscopy measurements were performed in air. This was done before and after 10 minutes of annealing at $140C$ in a nitrogen atmosphere in the glove box.

5.1.2 Absorption Spectroscopy

Working principle

When light, with an equal or higher energy than the bandgap of the polymer, illuminates on the sample, it promotes electrons residing in the HOMO to a higher energy orbital. Here, the absorption of light is exponentially related to the fraction of absorbing molecules encountered by the light, F. Secondly, it is also correlated with the thickness of the molecular layer $d(cm)$.

These two relationships are combined in the Law of Lambert-Beer, which given in equation

5.1

$$\frac{I_{detector}}{I_{lamp}} = 10^{(-\epsilon dF)} \tag{5.1}$$

Where I_{lamp} is the incident light intensity on the sample and $I_{detector}$ is the light intensity falling on the detector.

In general, a UV/Vis spectral setup, such as the Varian Carry 500 used during this thesis, is built up from 5 compartments as described in figure 5.1 [32][33]:

- First a stable source of radiant energy is needed. In most UV/Vis measurement setups, a continuum light source is used. The light in the visible range comes from a halogen lamp ($240-2500nm$). For ultra violet light, the system uses a deuterium-lamp ($160-380nm$).

- Wavelength selectors are used to isolate a limited region of the spectral range of the light source for measurement. This is necessary to restrict the radiation being emitted to a narrow band that is absorbed by the sample. In this way the chance for deviations from the law of Lambert-Beer due to polychromatic radiation is diminished. For UV-Vis measurements, monochromators are used as wavelength selector. It consists of a number of gratings to split white light in different energetic fractions. Besides this, there are also slits openings present at the entrance and exit of the setup. This is necessary to improve the wavelength selection. When the slit opening is smaller, the spectral shape leaving the setup will narrow. But by reducing the slit opening, the light intensity leaving the monochromator is also diminished. So there should be a good equilibrium between the light intensity leaving the monochromator and the spectral line broadening. The light used from the monochromator had wavelengths between 200 and 1000 nm. These were produced at a scanning speed of $1\frac{nm}{s}$ and a resolution of 1nm. Each measurement was integrated over a period of 1s.

- The sample compartment consist of a special designed sample holder. This was used to make these samples compatible with the UV-Vis setup.

- The detector consists of photo diodes. In many cases it is necessary to use multiple photo diodes with sensitivities to different spectral regions in the UV-Vis spectrum.
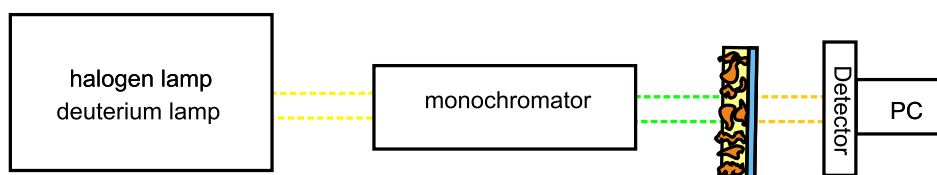
- The signal processing was done by a computer.

Figure 5.1: The setup for UV-Vis spectroscopy.

5.1.3   Fluorescence emission spectroscopy

Working principle

A fluorescence emission setup such as described in figure 5.2 is used. The light source used for spectrofluorimetry is a Xenon lamp. These lamps are very useful because of their high

intensity at all wavelengths ranging from 250nm up to 1000nm. An excitation monochromator is used to select the wavelength of the light falling on the sample. After the electrons of molecules are excited to higher energy levels by absorption of electromagnetic radiation, they will relax back to a more stable ground state by emission of a photon with an energy according to the energy difference between the excited- and the ground state. Since not all the lost energy is released as light, the wavelength of the fluorescent light is longer than that of the absorbed light. The emitted light is collected by an emission monochromator in an angle of 90 in respect to the exit of the excitation monochromator to prevent the detection of excitation wavelengths. Like absorption spectroscopy, fluorescence spectrofluorimeter monochromators also use slits to regulate the width of the energy distribution of the excitation and emission light. Afterwards the photons are converted in an electrical signal by the use of a photomultiplier tube which measures the number of photons per second falling on the photo anode. At last this electrical signal will be read out by a computer [32][33].
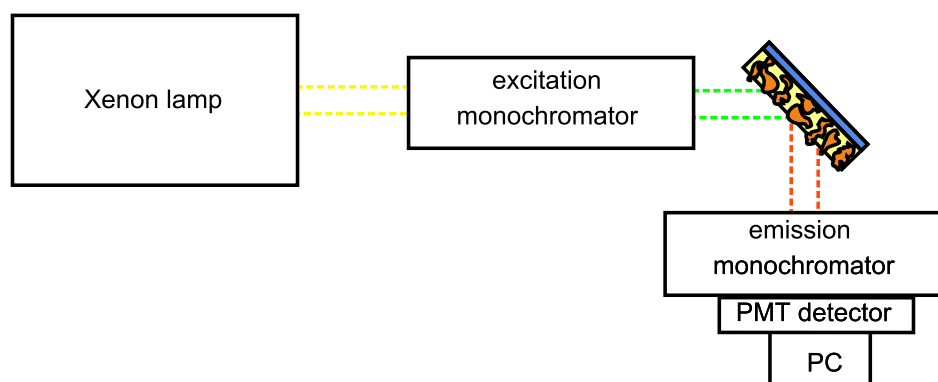
Figure 5.2: The setup for spectrofuorimeter.

For this thesis a Fluorolog Tau-3 Lifetime system is used. For good fluorescence spectra, the samples were excited at 375nm, and emission spectra were measured in the range of 400-750nm with a speed of $1\frac{nm}{sec}$. To measure the light intensities of the pure materials and the mixtures at the same slit opening, a slit opening of 1nm was used for both excitation and emission monochromators.

5.2 Atomic Force Microscopy

5.2.1 Working principle

The samples were prepared as described for the optical measurements. The only difference is that the dimensions of the samples were adapted to dimensions usable in the atomic force microscope (AFM).

Contact mode AFM is a method used to describe the topography of a surface in orders of nanometers to micrometers. For the measurement setup, a small tip is attached to a cantilever. This tip scans over the surface of the sample in one plane. When the tip encounters the material surface, interactions between atoms in the tip and those on the sample surface, related with the height of the sample and its chemical composition, creates a characteristic

force profile and cause eventual attraction or repulsion of the tip to the surface. A laser beam is bounced off the cantilever and directed toward a photo diode detector to record the deflection of the cantilever in response to the surface. In response to the change in deflection of the laser-signal a feedback loop is created towards a piezo-electrical crystal to adjust the sample position, and restore the deflection of the laser. This signal is related to roughness of the sample.

For polymers and other soft surfaces, contact mode is not useful because of the high risk to damage the surface of the sample. Therefore, the tip will oscillate during the measurements. This AFM-method is called tapping mode AFM. Apart from information about the surface morphology, it is now also possible to get a measure for the influence of the attractive forces of the surface on the cantilever oscillating frequency. If during the experiment the oscillation amplitude of the tip is kept constant by a feedback loop, it is possible to detect changes in the tip-sample interaction causing a modulation of the tapping frequency and consequently a phase difference between the input frequency and the recorded frequency. These signals will be processed by the use of a computer [34].

For the measurements a surface of $0.5m^2$ and $1m^2$ were measured using a Nanoscope IIIa AFM.
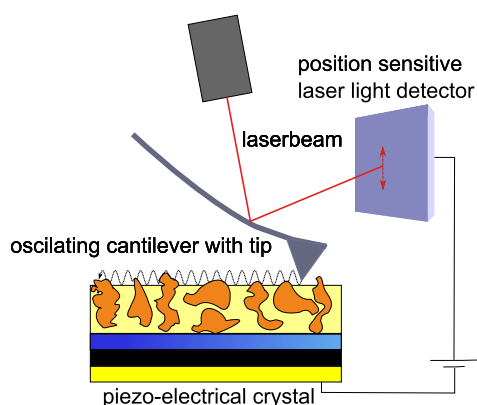
Figure 5.3: The working principle of tapping mode atomic force AFM.

5.3 Electrical techniques

5.3.1 Sample preparation

For making solar cells, glass with a conductive layer is needed. For this thesis, glass with an ITO-layer is used. These substrates were washed the same way as described in the section for the optical measurements. After washing, the substrates were placed under an UV-lamp for 15 minutes. This lamp will produce ozone, what will be used to burn remaining small organic molecules on the glass surface. Afterwards, a layer of PEDOT:PSS (HC. Stark) was deposited by spin coating in air (WS-400XB-6NPP/LITE). This layer annealed for 20 minutes at $120C$ on a hot plate.

The polymer blends were prepared in the same way as for the optical measurements. To prepare solar cells, the polymer was deposited on ITO:PEDOT-glass by spin coating. The

spin coat settings for the spin coater in the glove box (Karlsuss CT 62) were the same as described for the optical measurements to ensure that no morphological effects would interfere in the comparison between optical and electrical measurements.

After spin coating the polymer layers were deposited, a metal counter electrode was evaporated on this layer. This was done with a built in metal evaporator (Leybold). The evaporation process is done at ultra high vacuum ($1.6.10^{-6}mbar$). First, a 20nm Calcium (Calcium ingot 99% alfa Aesar) layer was deposited. Secondly a 50nm thick layer of Aluminium(99.9% Kurt J. Lesker company) was deposited.

For all measurements, these solar cells are kept in a nitrogen environment to prevent the oxidation of the calcium layer.

5.3.2   IV-characterization

The IV-characteristics of the solar cells were measured using Keithley 2400 source meter. The solar light was simulated using a Newport oriel class A solar simulator. This simulator produces a parallel light beam on the solar cell with a power of 1 sun at 1.5AM illuminating the solar cell. The current was measured at voltages from -0.5V up to 2V.

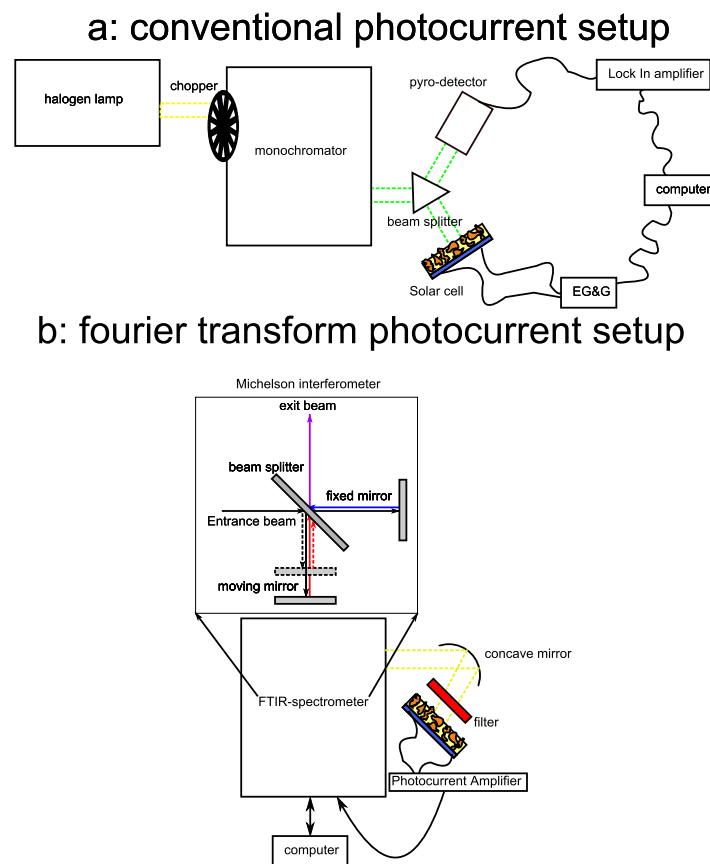### 5.3.3   Photo current measurements

For photocurrent (PC) measurements, the number of electrons per wavelength, impinging on the solar cell is measured. The setup is depicted in figure 5.4 (a). As a source of light a halogen lamp used, chopped at 20Hz by a wheel chopper. This light is split into different energy components by the use of a monochromator. This monochromatized light was focused up on a beam splitter to split it into two beams. One beam of light was directed to a pyro reference detector, connected with a Stanford Research System, model SR830 Lock-in amplifier. This lock-in measures the spectral response of the light source and serves as a reference measurement for the sample outputs. The other part of the light was focused onto the solar cell. If the light falling on the solar cell has enough energy, it will give rise to a photocurrent. This photocurrent was preamplified using a model 5182 Perking Elmer preamplifier. This signal was measured using a $EG\&G720$ lock-in amplifier. The two signals were sent to a computer system were they were processed using a homemade Labview program [26].

Another way to measure the photocurrent is called Fourier Transform Photocurrent spectroscopy (FTPS). A schematic representation of the setup is displayed in figure 5.4 (b) bottom. This method is based on the working principle of Fourier transform infrared (FTIR) spectrometer [26]. In FTIR, the source of light is modulated by a the Michelson interferometer instead of a monochromator. When an incoming beam of white light enters the interferometer, it will fall on a beam splitter used to split this light beam in two separate beams. One of these beams will be transmitted by the beam splitter and will fall on a fixed mirror, while the other will be reflected by the beam splitter in an angle of 90. This beam will fall on a moving mirror. This moving mirror moves between two fixed positions. Both of the mirrors will reflect this light beam back into the beam splitter. According to the wavelike nature of light and energy, the returning light beams will interfere with each other, because of differences in the path length that both waves have traveled to reach the beam splitter again. This interference can be constructive or destructive. The resulting outgoing beam will still consist of white light, but the fractions of energy present in the beam will be different according to

the position of the moving mirror. This outgoing light is directed out of the spectrometer and focused on the solar cell, generating a photocurrent. The amount of this photocurrent produced is dependent of the spectral response of the solar cell, and also on the path length difference of the light beams in the interferometer. By the use of a Fourier transformation, it is possible to convert the signal dependent on the path difference into an energy (in wave number) dependent signal using:

$$I(\nu) = \int_{-\infty}^{+\infty} I(\delta)cos(2\pi\nu\delta)d\delta \tag{5.2}$$

Where ν is the wave number expressed in cm^{-1} and δ is the difference in path length between the two rays [21].

Figure 5.4: The working principle of photocurrent. (a) The conventional setup for photocurrent measurements. (b) The setup for FTPS measurements.

Chapter 6

Result and discussion

6.1 Atomic force microscopy

6.1.1 Height profile measurements

The AFM-measurements show that the topography of the surface of a PFB:F8BT (1:1) blend gets rougher after annealing for 10 minutes at a temperature just above the glass temperature of F8BT (140C [35]) (figure 6.1). The increase in roughness is probably caused by a rearrangement of the polymer chains.
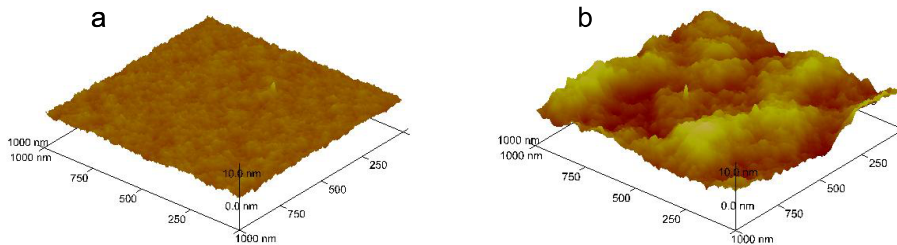
Figure 6.1: Comparison of the topography of a F8BT:PFB (1:1) blend sample surface (a) before and (b) after annealing for 10 minutes at 140C.

As shown in figure 6.2 the root mean square (RMS) of the height positions is used as a measure for the roughness of the surface of the sample. It can be seen that the RMS increases over all blends after annealing. Where the unannealed blends show only a minor increase in roughness with fraction of F8BT, the RMS value for the annealed films increase by a factor of 10 orders of measurement for fractions of F8BT rising from 0 till 0.6. Although the increase in roughness is seen, the films are is still relatively flat (1.8nm). For the ranges of F8BT:PFB fractions higher than 0.6, the RMS drops again. From the roughness data, no surface structure was evident. Because the sample was measured in tapping mode, it was also possible to extract information from the phase difference in the samples before and after annealing. These measurements will be discussed next.
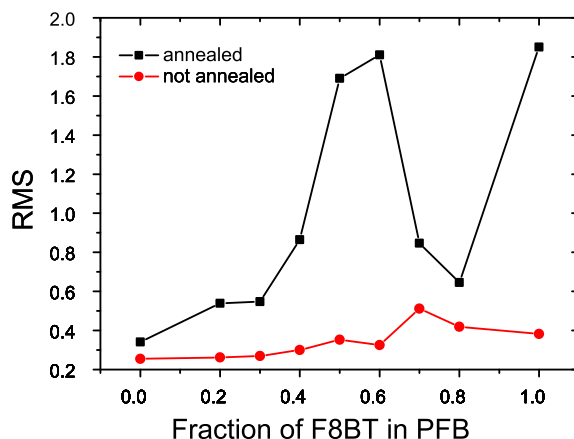
Figure 6.2: Comparison between the root mean square (RMS) on the topography of the sample for
F8BT:PFB spincoated films of fractions ranging from 0-1 F8BT in PBF.

6.1.2   Phase measurements

In figure 6.3 the phase images of all films are displayed before and after annealing. It can be
seen that before annealing, there is no phase separation visible. Also, after annealing, there is
no difference in phase image with the unannealed sample for pure PFB. But when the fraction
of F8BT in the blends rises, it can be observed that after annealing small islands are forming
(2'). When the fraction of F8BT compared to PFB keeps rising, this nodular structure evolves
into extended fiber like morphologies (5'-6'). This effect goes hand in hand with the increased
surface roughness. In figure 7' till 9' the fibers are still there, but the roughness diminishes.
This is probably caused by a decrease in the fraction of PFB. Since for pure F8BT the film
morphology changes upon annealling to result in a fiber like microstructure that is generic
for all annealed films with a fraction > 0.4 F8BT in PBF, it can be suggested that F8BT
chain rearrangement is the driving force for the microstructural changes observed. This is
in analogy to the findings published in the following publications [29] [36] [37]. Deviations
from the exact phase separated morphology published in these articles are due to the large
discrepancy in molecular weights of F8BT used in the publications and in this work.
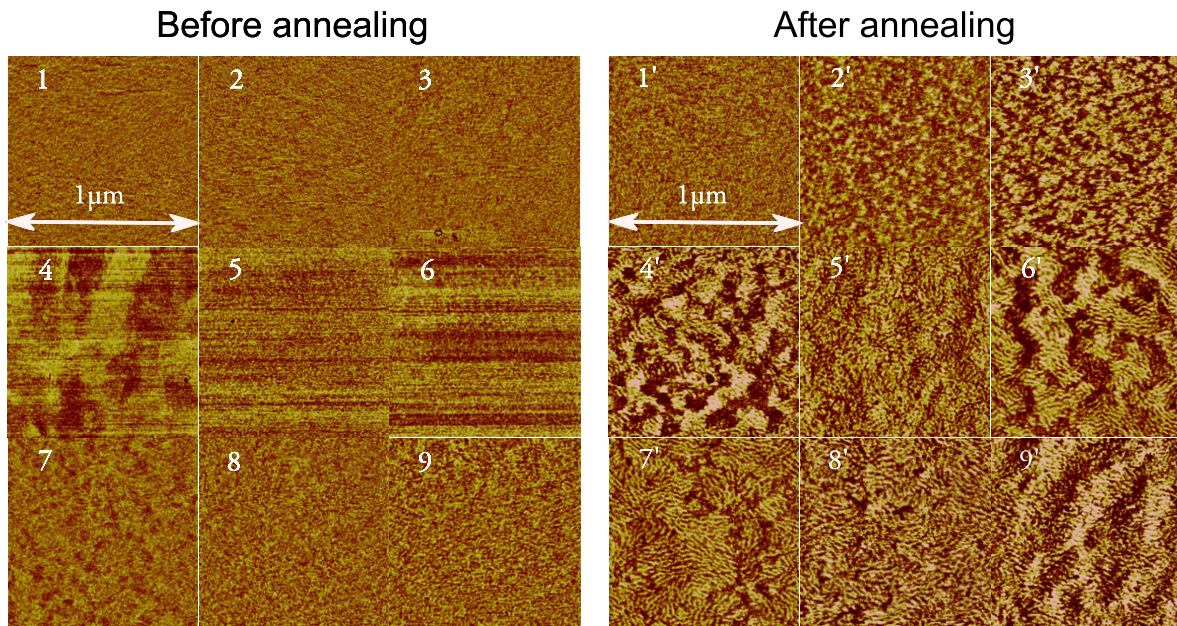
Figure 6.3: Comparison of the phase separation of the samples before and after annealing. $(1-9)$ are the phase pictures of the samples before annealing with an increase in F8BT fraction (1-9,0-1 F8BT fraction respectively). $(1'-9')$ are pictures of the same samples after annealing for 10 minutes at 140C.

6.2 UV-Vis absorption spectroscopy

6.2.1 Absorption measurements

In figure 6.4, the absorption spectra of the pure materials and blends of F8BT in PFB (0.2-0.8 F8BT) before and after annealing are shown. It is possible to see that the peak around 476 nm rises with the fraction of F8BT. This is the transition from the ground state to the first excited state, also called the zeroth order transition. At the same time the contribution of the peak, related with zeroth order transition of PFB (at 381nm) drops with the reduction in the fraction of PFB. The peaks around 300-350 nm are contributions of transitions of F8BT from the ground state to higher excites states. These are called also higher order transitions. This is confirmed in [36] [37].
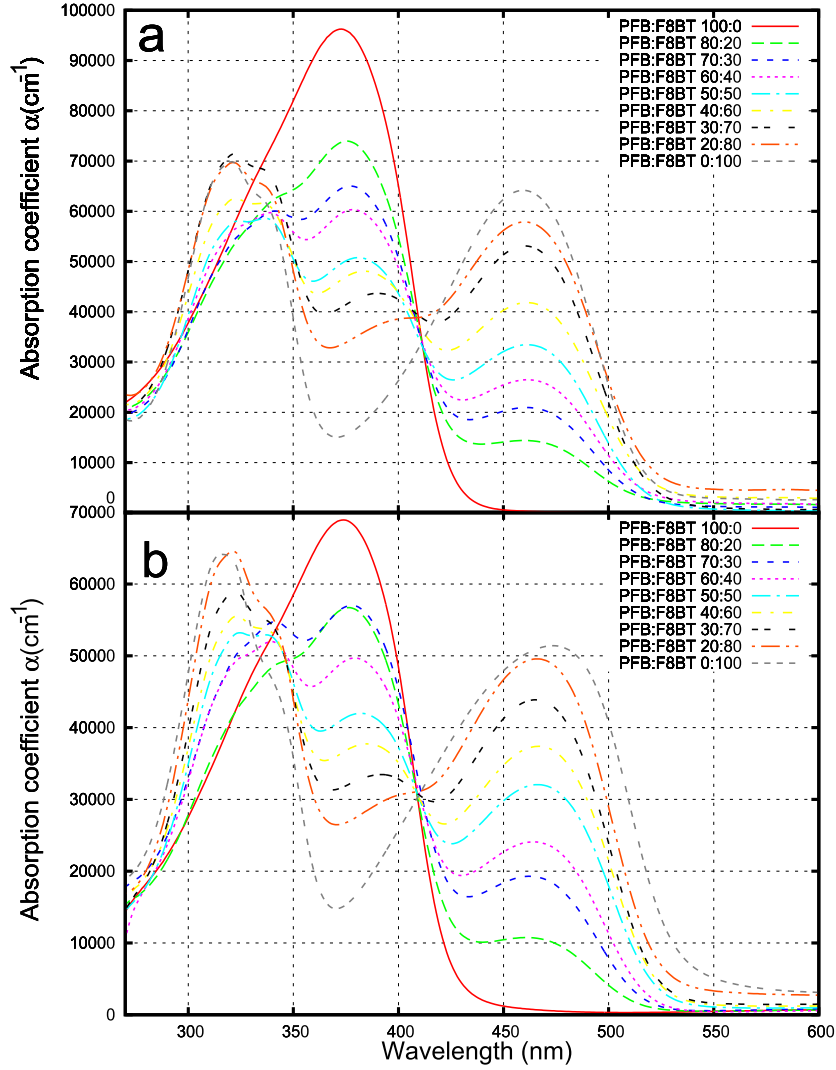
Figure 6.4: Comparison of the absorption spectra before (a) and after (b) annealing for 10 minutes at 140C.

The spectra were modeled with Gaussian functions for the transitions from the ground state to the first excited state and Lorentzian functions for the transitions between the ground and higher excited states. Since there is significant overlap of the absorption peaks of the composite spectra, a mathematical procedure was applied to improve the resolution of the peaks to be modeled. The equation describing the the Gaussian relation is given in equation 6.1:

$$A(E) = A_0 exp(\frac{-(E - E_c)^2}{2\sigma^2})$$ (6.1)

Here A_0 describes the amplitude of the Gaussian distribution, E_c the central energy and σ is a measure for the peak width.

For the Lorentzian distributions the following equation was used:

$$A(E) = y_0 + \frac{2 * A_0}{\pi} \frac{\sigma}{4 * (E - E_c)^2 + \sigma^2}$$ (6.2)

Where y_0 is the height of the base line.

To understand the role of resolution enhancing in the peak modeling, it is of great importance to understand the mathematics behind it [38]. As can be seen in figure 6.5, the first derivative is a good measure for the slope of the original function.
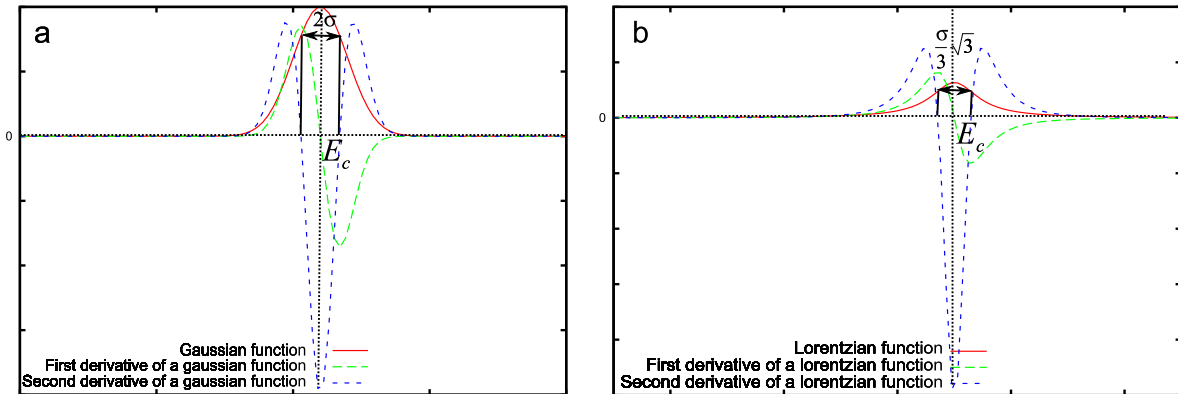

Figure 6.5: Effects of differentiation on Gaussian (a) and Lorentzian (b) functions

If the first derivative is positive, the slope of the original data is positive, and when the first derivative is negative, the slope of the original function is also negative. The maximal y-value of the original function is thus on the same x-position where the first derivative is equal to zero (E_c). The second derivative is a measure for the inflection of the original curve. In the maxima of the original curves, the inflection is also maximal. On the places where in the second derivative is zero, the inflection is also zero. The latter points are very useful to find the width of the peaks. The distance between the two point where $x = 0$ in the second derivative is equal to 2σ for Gaussian functions and $\frac{\sigma}{3}\sqrt{3}$ for Lorentzian ones. Here, σ is a measure for the peak width.

In figure 6.6 the second derivative of the absorption spectra of figure 6.4 are shown. It can be seen that the positions for maximal energy of the zeroth order transitions for F8BT and PFB are not well defined. This is possibly caused by thermal broadening. This leads to a number of small Lorentzian peaks in close proximity to each other. The existence of these small peaks can be explained quantum mechanically according to the density of vibrational states in the materials. This gives the possibility make a summation of the different Lorentzian peaks giving rise to a Gaussian like broadening of the curve [39]. The higher order transitions of F8BT are better defined. It can be seen in figure 6.6 that in the region between 300 and 350 nm, three different peaks are present, which can be modeled by Lorentzian functions.
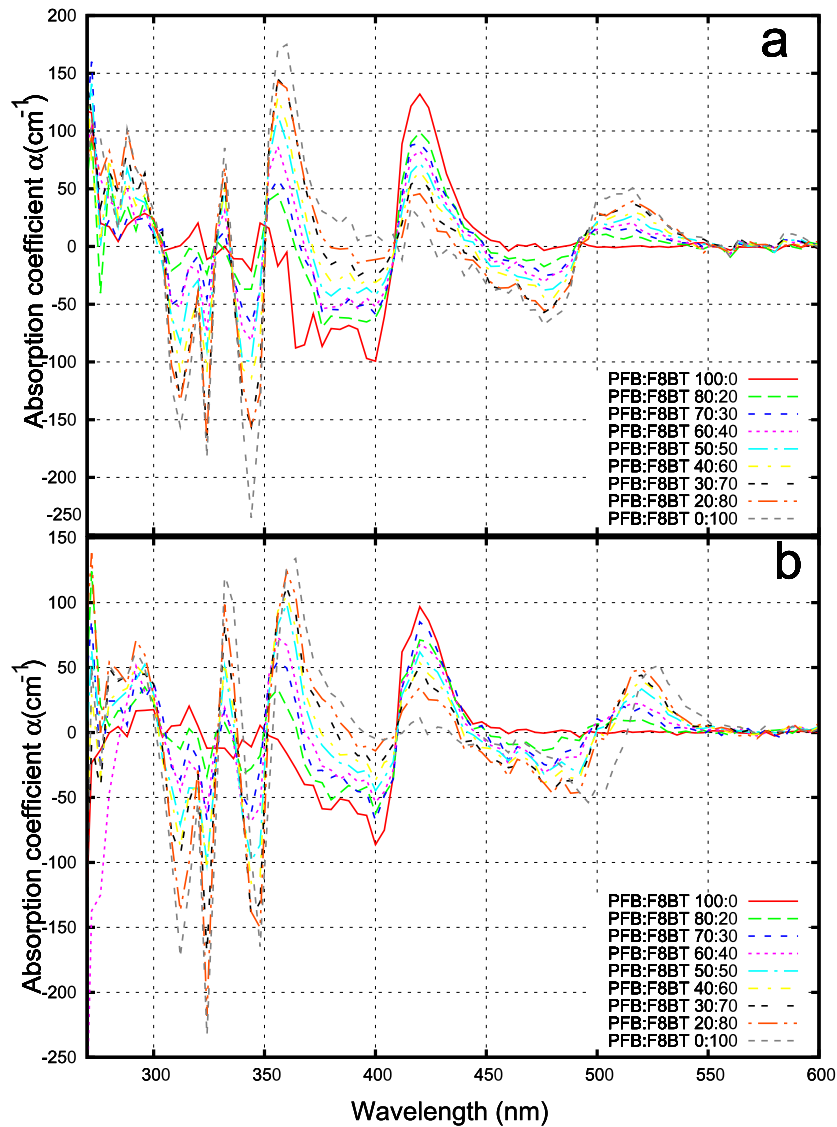
Figure 6.6: Comparison of the second derivative of the for thickness corrected the light absorption spectra before (a) and after (b) annealing for 10 minutes at 140C.

The fitting procedure can be described as follows: from the data present in the second derivate, the peak positions and the intersections with the x-axis were defined. Afterwards, the obtained values were used as starting values for the curves presented in figure 6.4. Here, first of all the amplitudes of the different peaks in the curve were modeled while the peak widths and central energies were kept constant. After this was done, the values of the peak widths were adapted to obtain a good fit. For the peaks corresponding to PFB (around 381 nm) and F8BT (around 476nm), the central energy was also corrected using the real spectra displayed in figure 6.4. In figure 6.7, the results of this fitting procedure are displayed. This figure represents the other fits made for the absorption spectra. From the fit parameters, it was possible to calculate the area under the curve (AUC) which are described in the figure 6.8.
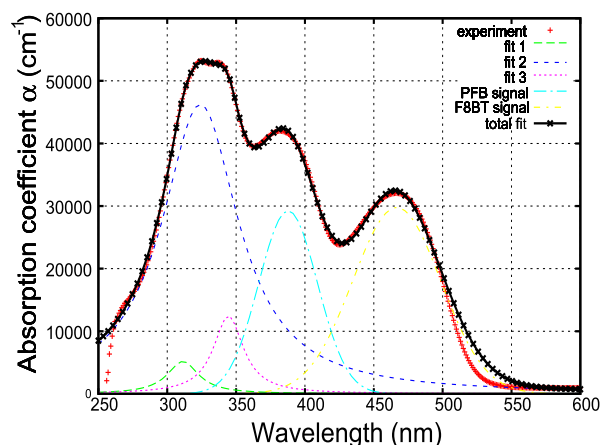
Figure 6.7: The result of curve fitting in 50:50 mixture of PFB:F8BT after annealing. The first three peaks in the wavelength range from 250nm till 350nm, are transitions of the electrons between the ground state and higher excitation states. The two peaks at lower energy are from PFB (381nm) and F8BT (476nm).

From the fit parameters, it was possible to calculate the area under the curve (AUC). These are plotted in figure 6.8 against the fraction of F8BT in PFB. From this graph, we can see that there is a linear relation between the AUC and the change in fraction. This means that our films are of perfect quality and no electrical interactions occurs between F8BT and PFB within the ground state.
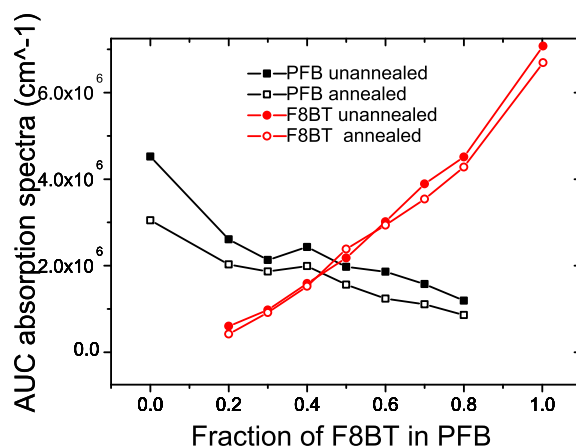
Figure 6.8: The AUC calculated from the fitting-parameters of the PFB-peak and F8BT-peak at different concentrations. This was done for the results before and after annealing. 6.7.

6.2.2   Fluorescence emission spectroscopy

In figure 6.9, the fluorescence spectra of pure materials and blends of F8BT and PFB (0.2-0.8 with steps of 0.1) are shown. To compare the emission signals of the pure samples with the blends, the samples were all measured at a slit width of 1nm. Therefore, the noise on the

signal of the blends is relative high compared to the absorption data. It can be seen for the PFB-signal (450nm), that a large amount of the fluorescence signal is quenched even when small fractions of F8BT (e.g. 80:20 PFB:F8BT) are present. The peak around 541 nm is due to F8BT and rises with increasing the fraction of F8BT. The shoulder above 652nm is possibly due to exciplex fluorescence and has been observed previously by Gonzalez et al. Here they studied similar polymer combinations and detected exciplex emission at 630nm [30].
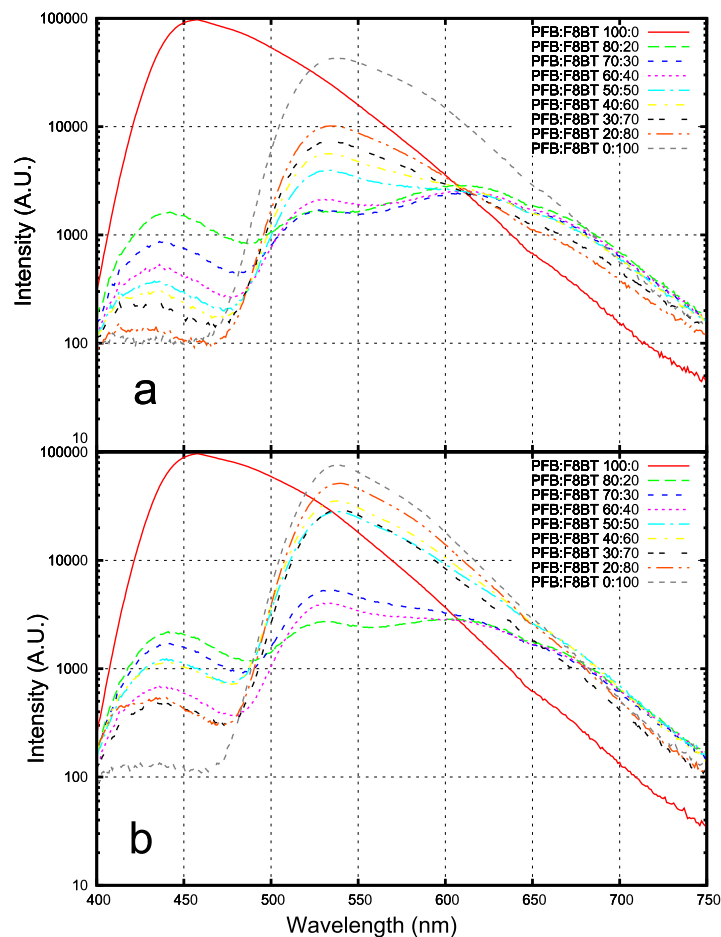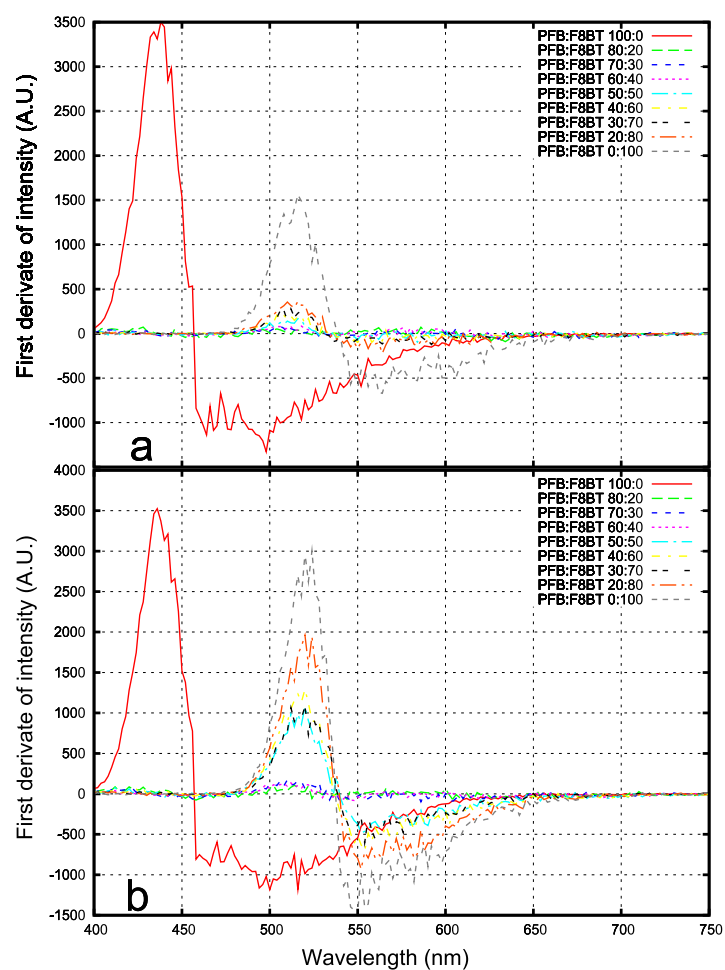

Figure 6.9: Emission spectra before (a) and after (b) annealing for 10 minutes at 140C.

It can also be seen that the amount of PFB-fluorescence after annealing is more or less similar to the intensity before annealing. The F8BT-fluorescence intensity, on the other hand, undergoes a big increase in fluorescence signal. This can be explained by the rearrangement of F8BT polymer chains in ordered domains with a more planar parallel conformation as a result [35]. This result is in accordance with our previous AFM descriptions, where a F8BT fiber like morphology was observed.

These spectra were also processed using the same method as described in the section of the absorption measurements. The $\frac{signal}{noise}$-ratio was very low for the second order derivation, so the information used was extracted from the first derivate of the signal described in figure

6.10.

Figure 6.10: First order derivation of emission spectra before (a) and after (b) annealing for 10 minutes at 140C.

The spectra of the pure materials dominate figure 6.10 and therefore hide the details of the blended spectra. Moreover, the noise on the blended signal was also quite high. So a Bezier-smoothening was performed on the first derivates of the measurement. These results give rise to a more useful picture given in 6.11, where the spectra of the pure materials are omitted for clarity.
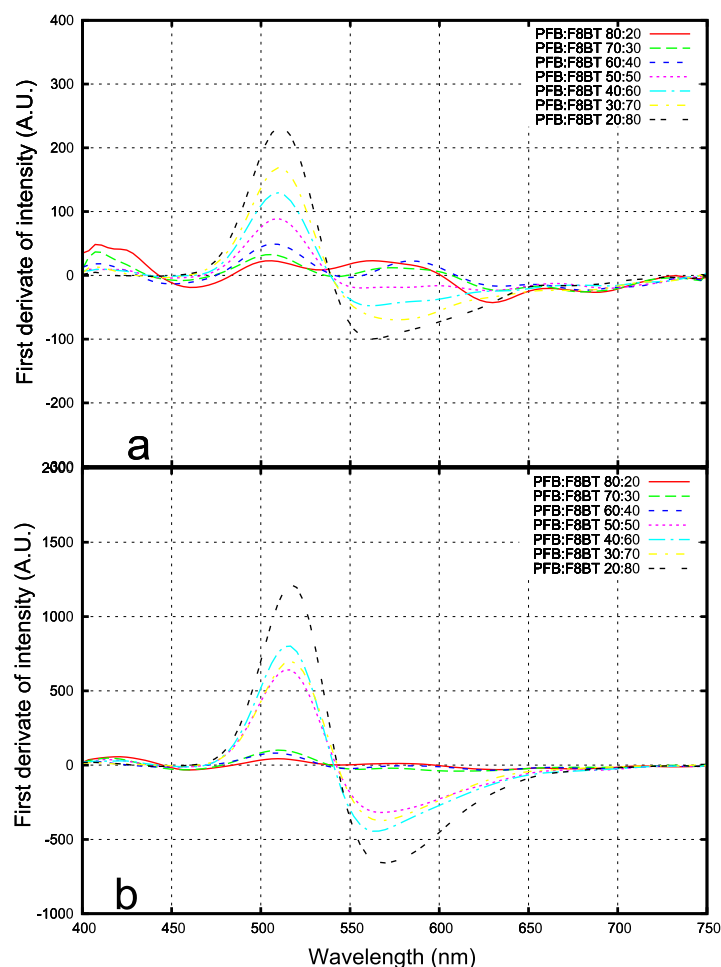
**Figure 6.11:** Bezier smoothened first order derivation of emission spectra of the blends before (a) and after (b) annealing for 10 minutes at 140C.

From these results, it can be seen that there are no extra peaks present in the spectra besides those already seen in the original data. Due to the weak exciplex emission intensity in respect to the emission of F8BT, this signal is hardly observed in the first derivate of the spectra.

Peaks according to the zeroth transition of PFB/F8BT are fitted using Gaussian functions, while the extra peak is fitted using a Lorentzian function. There was a problem with the pure materials because the first derivative of the signal could not be fitted to the first derivative of Gaussian or Lorentzian functions. Therefore these curves were fitted using an asymmetric double sigmoidal function. The broadening towards the low energy part of the spectrum is possibly due to the presence of a high number of density of vibrational states in the upper part of vibrational levels in the ground state.

These tail like structures were not as explicit present in the mixtures with high PFB:F8BT-fractions . When the fraction of F8BT rises, these tail like structures began to occur, but it was still possible to fit these data using Gaussian and Lorentzian functions. In figure 6.12, a representative result of the curve fitting procedure is displayed.
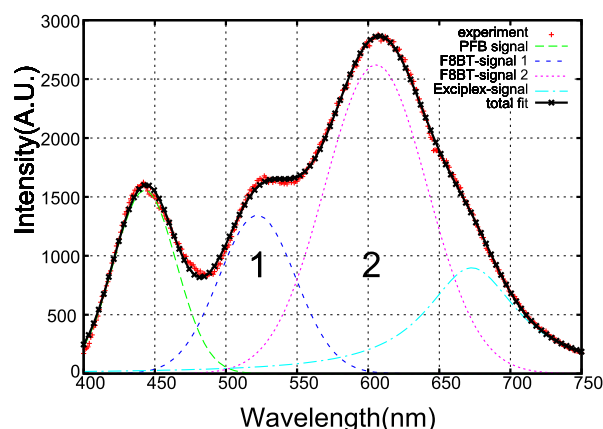
Figure 6.12: The result of curve fitting of the emission signal in a 80:20 blend of PFB:F8BT before annealing. The peak related to PFB is represented by the green curve. The peaks labeled with 1 and 2 are both related to F8BT.

The AUC related to the emission of F8BT and PFB as a function of F8BT fractions in blends before and after annealing is plotted in figure 6.13. When looking to the fluorescence of PFB relatively to the fluorescence signal produced by F8BT, it can be seen that the signal corresponding to PFB is lower than that of F8BT. The fluorescence intensity is influenced by the chemical composition of the polymer and the molecular weight. Moreover the local microstructure can affect this [35]. To illustrate the exact interplay of these effects, further research in necessary.
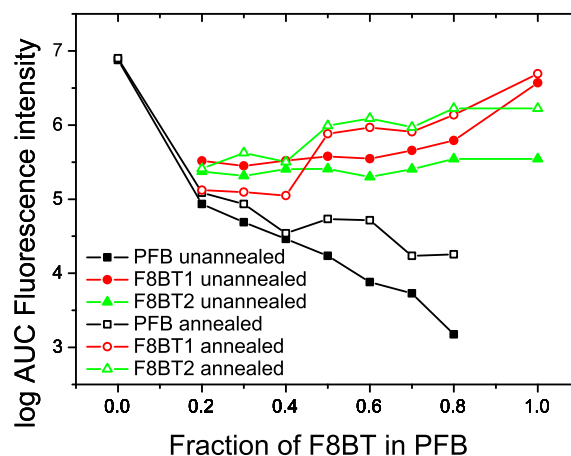
Figure 6.13: The result of curve fitting of the emission signal in a 80:20 blend of PFB:F8BT before annealing.

We observe that the fluorescence intensity after annealing rises in both F8BT and PFB. If the fraction of F8BT:PFB rises above 0.5, a general increase in fluorescence is observed.

The fluorescence signal of pure PFB is 2 orders of magnitude higher than when PFB is present in a blend. For F8BT, this difference is less visible, due to the spread of the area be-

tween the two peaks. This quenching effect proves that the material combination is promising for the use in organic solar cells, since it is indicative for the efficiency of free charge carrier generation. The quenching process can be caused by energy- or electron transfer. When electron transfer is favoured free holes and electrons are generated and give rise to photocurrent. It is also visible that the fluorescence intensity in the annealed samples is relatively higher compared to the unannealed samples. This is related with aggregate formation after annealing of F8BT:PFB blends as observed with AFM, decreasing the interfacial area between the two components and therefore the photoluminescence quenching probability. The formation of more rigid and planar molecular chains play a role in increasing the fluorescence intensity [35] [32].

From the cyclic voltametry measurements published in [30], it is seen that the energy difference between HOMO and LUMO of the electron donor PFB is equal to 2.92eV. The difference between HOMO and LUMO of the acceptor F8BT there is equal to 2.6 eV. These values are in the same range as the energy differences measured by absorption and emission measurements for which the values used are estimated by fitting the corresponding peaks in the spectra with Gaussian functions: 3.18eV and 2.69eV for PFB and F8BT respectively (e.g. 1:1 in absorption). Afterwards the E_c values for the annealed samples were subtracted from the E_c values of the unannealed ones. The results are plotted against the fraction of F8BT in the blend as can be seen in figure 6.14. Here in figure 6.14 it is seen that all the differences in E_c are positive. This indicates that both PFB and F8BT peaks are red shifted after annealing. From figure (a) it is possible to see that in the absorption spectra the peak position of PFB is almost unchanged after annealing. Just a shift of 0.014eV was observed. For F8BT, it can be seen that a red shift of 0.03eV has occurred during annealing. In figure 6.14 (b) the peak position for the emission spectra are presented. Here, it is seen that due to annealing, the PFB-emission peak is red shifted for 0.09eV. The F8BT peak on the other hand is red shifted with 0.03eV corresponding to the red shift seen for F8BT in the absorption bands.
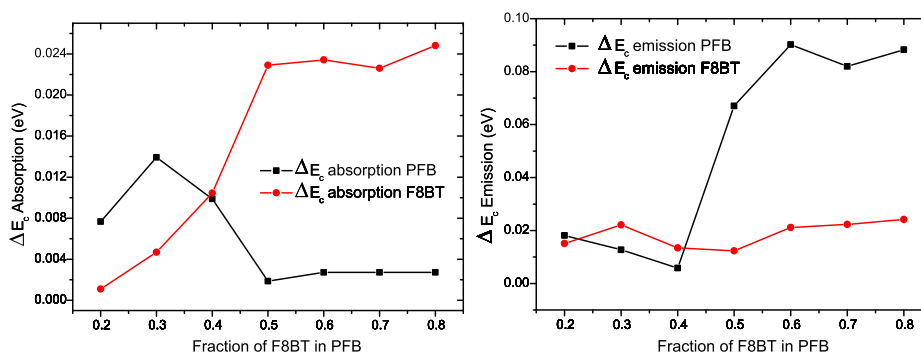
Figure 6.14: Here a comparison is made between the difference in peak position before and after annealing (ΔE_c) of the peaks of F8BT and PFB in (a) absorption- and (b) emission-spectra.

The general red shift in absorption and emission spectra is probably caused by the rearrangement of the polymer chains as was observed in the AFM-phase measurements. Before annealing, the F8BT- and PFB chains are intimately mixed with each other. After annealing

at the T_g of F8BT, small islands will emerge, consisting of aggregates of F8BT polymer chains. In these aggregates, extended conjugation within one phase will red shift the absorption and emission spectra. These phase separated region will gain slightly more absorption and emission characteristics of the pure materials, explaining the in increased emission intensities observed [35].

6.3 Electrical techniques

6.3.1 IV-characterization

In figure 6.15 an IV-characteristic of a F8BT:PFB blend is shown. For every data point an estimation of the power can be made using the following equation:

$$P = IV \tag{6.3}$$

After this estimation was made, the power could be plotted against the voltage (green line). In the region of the maximal power, the curve was fitted using a quadratic function. From this function, the maximal power point was estimated. An estimation of the current (I_{max}) and voltage (V_{max}) can be estimated.
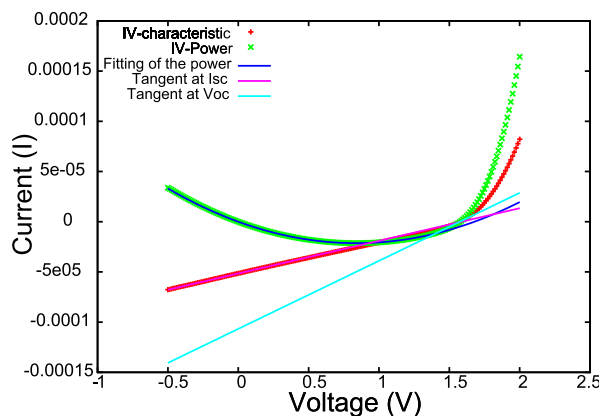
Figure 6.15: IV-characteristic of F8BT:PFB blend, together with it tangents at V_{oc} and I_{sc}, the IV-power function and a fitting of this function used to estimate the maximal power point.

The I_{sc} is estimated as the measurement-value were the voltage is nearest to 0V. The V_{oc} on the other hand is estimated as the measurement-value where the current is nearest to 0A.

After the estimation of these parameters, the fill factors (FF) and efficiencies (η) of the functions were calculated according the equations already considered in the introduction. The results for the F8BT:PFB blends before and after annealing, are given in figure 6.16.
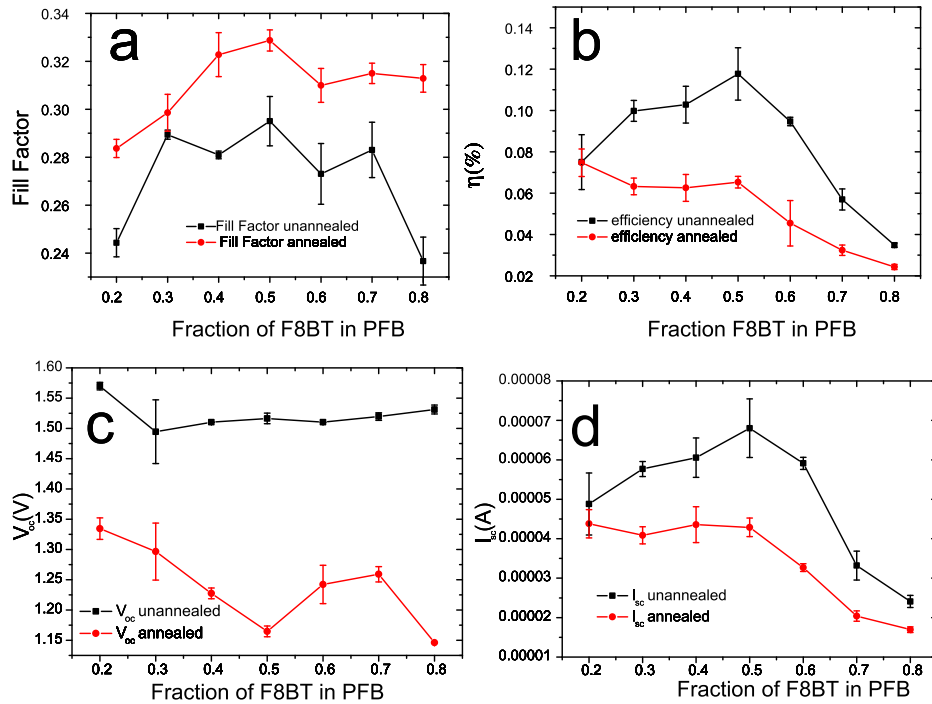
Figure 6.16: (a) Fill factor (FF), (b) efficiencies(η), (c) open circuit voltages (V_{oc}) and (d) short circuit current (I_{sc}) estimations of the solar cells made from different fractions of F8BT in PFB are represented here. The points in black represent the unannealed values, while the red points represent the values after annealing of the solar cells for 10 minutes at 140C.

We observed that the fill factor and efficiency of the solar cells rises till the fraction of F8BT in PFB is equal to 0.5. At higher fractions of F8BT, the fill factor and efficiency drop again. With fractions of F8BT in PFB, the V_{oc} of the corresponding solar cells decrease up to 0.5 to increase again at higher fractions (> 0.5). For the I_{sc} a reverse trend is observed. By combining these results, we can conclude that the fill factor and the generated I_{sc} dominates the efficiency trend observed. Also annealed cells give rise to higher fill factors, and therefore better diode quality (see chapter 4: Introduction). The maximal efficiency is measured in the 50:50 PFB:F8BT blend and is around 0.12%. This value drops to 0.065% after annealing of the same solar cell(figure 6.16 a). On the other hand it has been seen that the fill factor rises after annealing. This can be explained by a decrease in V_{oc} after annealing, leading to an increase in fill factor. A drop in $V_{o}c$ can be caused by a reduction of the LUMO level of the accepting material or an increase in the HOMO level of the donor material.

The drop in efficiency after annealing is correlated with the fluorescence data. If any relaxing electron can be considered as an electron that doesn't contribute to the photocurrent in the solar cell, it can be said that after annealing, the increase in the fluorescence signal of F8BT is related to the decrease in solar cell efficiency. This is also seen by Donley et All [35]. They explained this with quantum chemical calculations were, due to annealing, the F8BT polymer chains were aligned and planarized. By planarization, the ideal orientation for inter chain electron transport was lost, leading to less efficient charge transport and solar cells.
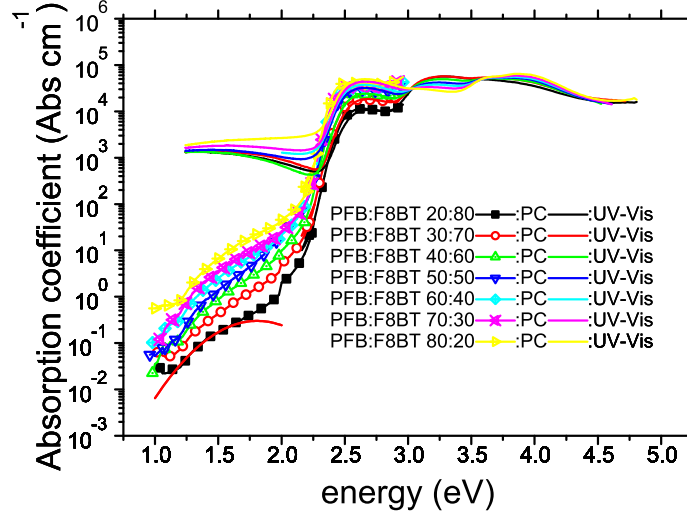
6.3.2 Photocurrent measurements

In figure 6.17 the photocurrent spectrum measured by FTPS is displayed. In the FTPS-plot (black curve) it can be seen that a tail is starting for energies beneath 2.5 eV, but the $\frac{signal}{noise}$-ratio is very low. This is possibly due to the fact that the FTPS measurements use high modulation frequencies (around 5kHz). So this technique can only be used on samples with fast photo responses. These slow photoresponses could be due to three major reasons. First of all, in PFB:F8BT solar cells the geminate pairs at the interface are strongly bound to each other, so that they need relatively more time to be separated than given in a period of $\frac{1}{5kHz}$. So the photocurrent-signal of this extra band is very low when it is measured using FTPS. Secondly, the mobility of the charge cafriers is low. Thirdly, fast recombinations can occur after charge separation at the interface. To see which effect dominates, it will be a subject of further investigation.
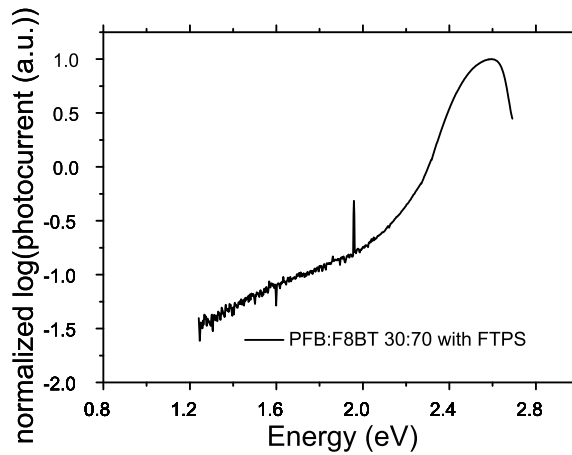
Figure 6.17: FTPS result of a PFB:F8BT blend with composition ratio 30:70.

To circumvent this problem, the photocurrent spectrum was measured with the conventional method, which uses monochromatic light chopped at low frequency (20 Hz). Because the exact number of photons falling on the solar cell and reference detector was difficult to control, the conversion of the signal to external quantum efficiency values was impossible to calculate. Normally, this can be done by correcting the signal for the spectral power of the lamp as can be seen from the introduction. To study whether this sub bandgap absorption feature is related with the interface properties of the material junction, we systematically investigated the fraction dependence of the photocurrent spectra. This was displayed in figure 6.18. The photocurrent signal (figures) has been corrected for concentration and layer thickness by relating them with the absorption coefficient (lines), measured by UV-Vis spectroscopy (see 5.2.1). In contrast with the conventional UV-Vis techniques, we were able to detect an extra absorption band from 1-2eV in the blend material. Such a transition has been observed before by L. Goris et al. and related to a ground state charge transfer complex (or exciplex). This absorption feature has proven to determine the effective gap and the V_{oc} of the solar cell [40]. We modeled this band using a Gaussian function as done for the PFB:F8BT 80:20 blend in the red curve in figure 6.18.

Figure 6.18: Photocurrent measurements performed by the conventional photocurrent method. These photocurrent data were calibrated to the absorption coefficient by aligning the spectra of F8BT:PFB blends of both measurements.

We observe a systematic increase of the magnitude of this band with increasing fractions of F8BT. It is however difficult to explain this behaviour as this property is determined by different factors. First of all, the interfacial area between donor and acceptor is important. Secondly, the oscillator strength of the transition will also influence the signal. Since these films have been annealed, the interfacial area is not a simple function of the fractions of the components, but depends also on the microstructure obtained. Moreover, the oscillator strenth can be influenced due to local changes in microstructure as well.

Moreover, the effective gap E_g from equation 6.1 of the photocurrent generation by CT-absorption was determined as:

$$E_g = E_c - 2\sigma \tag{6.4}$$

Like the V_{oc}, the E_g can be set out in function of the fraction of F8BT-blend with PFB as can be seen from figure 6.19. This shows that the E_g follows a decreasing trend with the fraction of F8BT, while the V_{oc} drops till a fraction of PFB:F8BT is 50:50. Afterwards the V_{oc} rises again, while the E_g keeps on dropping. This graph proves that in F8BT:PFB solar cells the V_{oc} is related with the effective gap of the material combination. This relationship seems to break down for fraction higher than 0.5. This effect could be due to the limited amount of solar cells measured in this population. We will investigate whether other effects than the E_g influence the V_{oc}.
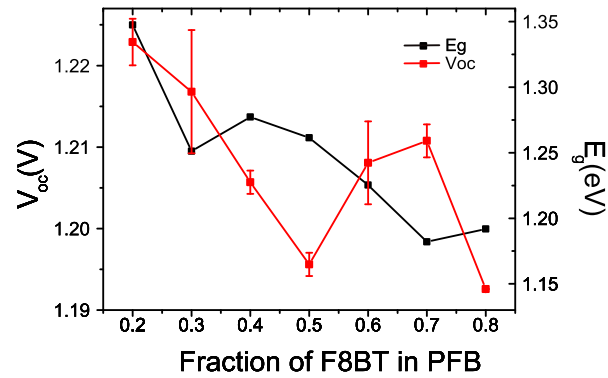
Figure 6.19: Concentration dependency of E_g and V_{oc} derived from conventional photocurrent and IV-characterization respectively.

It can be seen in figure 6.20, that during the illumination by bias UV-light, the peak between 1 and 2 eV disappears. This can be caused by the loss of present electrons in the CT-band when biased UV-light is emitted upon the sample. It is possible that this phenomenon can be generalized to all kinds of bias light, absorbable by the polymers, but further experiments are needed to confirm this.
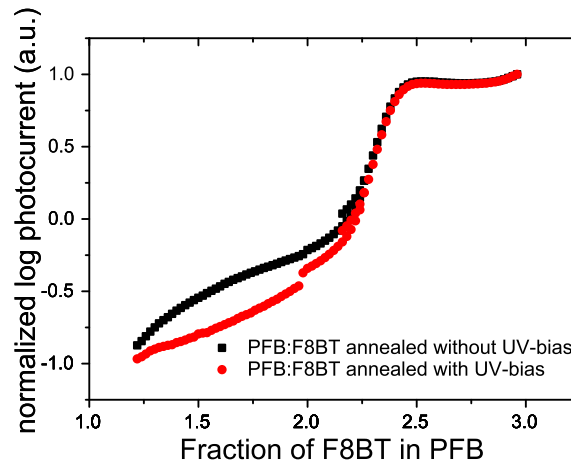
Figure 6.20: Normalized photocurrent spectra measured in the presence and absence of biased UV-light.

In the future, additional experiments will be performed to definitely exclude any degradation mechanisms that could interfere with the current interpretation of the results.

Chapter 7

Conclusion

From the beginning of photosynthetic life on Earth, originating from the first bacterial life forms, its working mechanisms have been adapted and tuned in such a way that life all over the world can use its benefits. Starting from the 1960's, mankind started to use the concept of photosynthesis for the development of artificial systems based on organic substances. Since then, a great variation of methods was developed to harvest solar energy by organic molecules. In this work, organic solar cells based on a donor-acceptor principle were investigated. The donor- and acceptor materials are respectively PFB and F8BT. These materials were blended in different fractions to investigate the fraction dependent properties of the resulting substances and solar cells. Also the effects of annealing at temperatures just above the glass transition temperature of F8BT were investigated.

The blends were investigated using a combination of morphologic, optical and electrical methods. The morphology was studied using AFM. This technique gave us the possibility to observe rearrangement of F8BT polymer chains in a fiber like morphology and gentle phase separation from the PFB molecules after annealing, increasing the roughness of the samples. Optical techniques were used to determine the behaviour of the absorption and emission properties of the materials and blends. For the unannealed samples a perfectly linear relationship was observed between the peak maxima of the pure materials in the blend absorption spectra as function of its fraction. Moreover, no additional absorption peaks are measured upon blending the materials. This indicates that no electronic interaction occurs in the ground state. However, fluorescence measurements gave evidence of the formation of an exciplex state in accordance with results previously published in literature. Since this species is an intermediate state that exists between the interface of the donor and acceptor components, we have investigated the blends with highly sensitive photocurrent techniques. By the use of highly sensitive photocurrent measurements a sub bandgap absorption signal has been observed in the range between 1 and 2 eV, most probably related to the formation of a charge transfer state (or exciplex) in the blend.

It has been seen that the annealing of F8BT increased the fluorescence intensities of F8BT after annealing. This is probably caused by a rearrangement of the polymer chains as was described by AFM. The observed red shift of the absorption and emission confirm this. With electrical techniques it has been seen that the overall efficiency of the solar cells lies around 0.12%.

Like for the processes in nature, there is always space for adaption and improvement of

the system. Also the understanding of the processes in the polymer solar cell presented in this thesis can be improved in order the increase the efficiency of these cells. Some points of discussion are presented in the list below

- The effects of bias-light on the solar cell have to be investigated further, in order to determine the photo-electrical properties of the sub-bandgap phenomenon. Also the effects of solar cell degradation on the absorption and emission of light. The solar cell performance and its influence on the sub-bandgap spectral features will be investigated.

- PDS measurements will be done to confirm the results obtained by photocurrent spectroscopy. Therefore the set-up will be equipped with a dual light source, to extend the working range below the bandgap.

- Due to annealing, the fluorescence intensity of F8BT rises a lot. Charge mobility measurements can be used to determine the effects of annealing on the mobility of electrons and holes through the polymers.

- After annealing, a reduction in the V_{oc} has been observed after annealing combined with a red shift of the peaks measured by absorption and emission spectroscopy. This is caused by a change in the electronic distribution in these solar cells. In order to investigate the binding energies of the electrons in the different bands, XPS-measurements can be applied.

- Until now, only steady state optical measurements were applied on this polymer combination. But according to Strickler and Berg, these steady state results are related with time-dependent processes. In order to get a better understanding of these solar cells, time dependent measurements have to be applied for the energies corresponding to the different peaks according to PFB, F8BT and the sub-bandgap phenomenon.

- To determine if the quenching of the fluorescence signal of PFB in the presence of F8BT is caused by energy transfer or electron transfer, it is possible to use advanced spectroscopic techniques such as photo induced electron spin resonance. These techniques are able to detect specific absorption bands of spins related to charge carriers (polarons) generated under the influence of illumination, and exclude energy transfer as possible quenching mechanism.

Bibliography

[1] T. Kelly and M. Wolf, "Template approaches to conjugated polymer micro- and nanoparticles," *Chemical Society Reviews*, vol. 39, no. 5, pp. 1526–1535, 2010.

[2] H. S. Nalwa, "Organic materials for Third-Order nonlinear optics," *Advanced Materials*, vol. 5, no. 5, pp. 341–358, 1993.

[3] M. Hmyene, A. Yassar, M. Escorne, A. Percheron-Guegan, and F. Garnier, "Magnetic properties of ferrocene-based conjugated polymers," *Advanced Materials*, vol. 6, no. 7-8, pp. 564–568, 1994.

[4] E. Aharon, A. Albo, M. Kalina, and G. Frey, "Stable blue emission from a polyfluorene/layered-compound guest/host nanocomposite," *Advanced Functional Materials*, vol. 16, pp. 980–986, May 2006.

[5] E. Moons, "Conjugated polymer blends: linking film morphology to performance of light emitting diodes and photodiodes," *Journal of Physics-Condensed matter*, vol. 14, pp. 12235–12260, Dec. 2002.

[6] J. Scott and L. Bozano, "Nonvolatile memory elements based on organic materials," *Advanced Materials*, vol. 19, pp. 1452–1463, June 2007.

[7] L. Pettersson, F. Carlsson, O. Inganas, and H. Arwin, "Spectroscopic ellipsometry studies of the optical properties of doped poly(3,4-ethylenedioxythiophene): An anisotropic metal," *Thin Solid Films*, vol. 313, pp. 356–361, Feb. 1998.

[8] G. Dennler, M. C. Scharber, and C. J. Brabec, "Polymer-Fullerene Bulk-Heterojunction solar cells," *Advanced Materials*, vol. 21, no. 13, pp. 1323–1338, 2009.

[9] F. Feng, F. He, L. An, S. Wang, Y. Li, and D. Zhu, "Fluorescent conjugated polyelectrolytes for biomacromolecule detection," *Advanced Materials*, vol. 20, pp. 2959–2964, Aug. 2008.

[10] A. J. Heeger, A. G. MacDiarmid, and H. Shirakawa, "The nobel prize in chemistry, 2000:Conductive polymers," 2000.

[11] L. Boltzmann, "Weitere studien über das wärmegleichgewicht unter gasmolekülen," *Sitzungsberichte der Akademie der Wissenschaften, Mathematische-Naturwissenschaftliche Klasse*, vol. 3, no. 51, pp. 275–370, 1872.

[12] P. M. Fishbane, S. Gasiorowicz, and S. Thornton, *Physics: for Scientists and Engineers with Modern Physics, Third Edition*. Benjamin Cummings, 3 ed., June 2004.

[13] T. C., *Fundamentals of Quantum Mechanics: For Solid State Electronics and Optics.* Cambridge University Press, 1st ed., 2005.

[14] P. WURFEL, "the chemical potential of radiation," *Journal Of Physics C-Solid State Physics*, vol. 15, no. 18, pp. 3967–3985, 1982.

[15] W. H. Armytage, *A Social History of Engineering.* Westview Press, 1976.

[16] C. Burdeau and M. Holbrook, "Expert: Surface area of gulf oil spill has tripled," *Edmonton Sun*, May 2010.

[17] M. Gratzel, "Solar energy conversion by dye-sensitized photovoltaic cells," *Inorganic Chemistry*, vol. 44, pp. 6841–6851, Oct. 2005.

[18] TRIBUTSC.H, "Reaction of excited chlorophyll molecules at electrodes and in photosynthesis," *Photochemistry and Photobiology*, vol. 16, no. 4, pp. 261–&, 1972.

[19] F. Gao, Y. Wang, J. Zhang, D. Shi, M. Wang, R. Humphry-Baker, P. Wang, S. M. Zakeeruddin, and M. Gratzel, "A new heteroleptic ruthenium sensitizer enhances the absorptivity of mesoporous titania film for a high efficiency dye-sensitized solar cell," *Chemical Communications*, no. 23, pp. 2635–2637, 2008.

[20] "Solarmer energy hits 7.9% efficiency with plastic solar cells." http://cleantech.com/news/5372/solarmer-energy-hits-79-efficiency.

[21] K. Vandewal, "charge transfer complexes in polymer:fullerene bulk heterojunction solar cells," 2009.

[22] M. Stomp, J. Huisman, L. J. Stal, and H. C. P. Matthijs, "Colorful niches of phototrophic microorganisms shaped by vibrations of the water molecule," *International Society for Microbial Ecology Journal*, vol. 1, pp. 271–282, July 2007.

[23] N. Y. Kiang, J. Siefert, Govindjee, and R. E. Blankenship, "Spectral signatures of photosynthesis. i. review of earth organisms," *Astrobiology*, vol. 7, no. 1, pp. 222–251, 2007.

[24] A. Einstein, "Zur quantentheorie der strahlung," *Phyzikalisches Zeitschrift*, vol. 18, pp. 121–128, 1917.

[25] S. J. Strickler and R. A. Berg, "Relationship between absorption intensity and fluorescence lifetime of molecules," *The Journal of Chemical Physics*, vol. 37, no. 4, p. 814, 1962.

[26] L. Goris, "Highly sensitive spectroscopic study of sub-bandgap absorption phenomena in organic thin film solar cells," 2009.

[27] A. Moliton and J. Nunzi, "How to model the behaviour of organic photovoltaic cells," *Polymer International*, vol. 55, no. 6, pp. 583–600, 2006.

[28] M. Lecler and M. Lecler, "Polyfluorenes: Twenty years of progress," *Journal of Polymer Science Part A: Polymer Chemistry*, vol. 39, no. 17, p. 28672873, 2001.

[29] C. McNeill, S. Westenhoff, C. Groves, R. Friend, and N. Greenham, "Influence of nanoscale phase separation on the charge generation dynamics and photovoltaic performance of conjugated polymer blends: Balancing charge generation and separation," *Journal Of Physical Chemistry C*, vol. 111, pp. 19153–19160, Dec. 2007.

[30] A. Gonzalez-Rabade, A. C. Morteani, and R. H. Friend, "Correlation of heterojunction luminescence quenching and photocurrent in Polymer-Blend photovoltaic diodes," *Advanced Materials*, vol. 21, no. 38-39, pp. 3924–3927, 2009.

[31] B. C. Thompson and J. M. J. Fréchet, "Polymer-Fullerene composite solar cells," *Angewandte Chemie International Edition*, vol. 47, no. 1, pp. 58–77, 2008.

[32] P. R. Reed, D. D. A. Holmes, D. J. Weyers, and D. A. Jones, *Practical Skills in Biomolecular Sciences*. Prentice Hall, 2 ed., Feb. 2003.

[33] D. A. Skoog, D. M. West, F. J. Holler, and S. R. Crouch, *Fundamentals of Analytical Chemistry*. Thomson brooks/colel, 1 ed., Jan. 2003.

[34] J. S. Temenoff and A. G. Mikos, *Biomaterials: The Intersection of Biology and Materials Science*. Prentice Hall, 1 ed., Jan. 2008.

[35] C. L. Donley, J. Zaumseil, J. W. Andreasen, M. M. Nielsen, H. Sirringhaus, R. H. Friend, and J. Kim, "Effects of packing structure on the optoelectronic and charge transport properties in poly(9,9-di-n-octylfluorene-alt-benzothiadiazole)," *Journal of the American Chemical Society*, vol. 127, no. 37, pp. 12890–12899, 2005.

[36] H. J. Snaith, A. C. Arias, A. C. Morteani, C. Silva, and R. H. Friend, "Charge generation kinetics and transport mechanisms in blended polyfluorene photovoltaic devices," *Nano Letters*, vol. 2, pp. 1353–1357, Dec. 2002.

[37] H. Snaith and R. Friend, "Morphological dependence of charge generation and transport in blended polyfluorene photovoltaic devices," *Thin Solid Films*, vol. 451, pp. 567–571, Mar. 2004.

[38] L. Antonov and D. Nedeltcheva, "Resolution of overlapping UV-Vis absorption bands and quantitative analysis," *Chemical Society Reviews*, vol. 29, pp. 217–227, May 2000.

[39] A. Tokmakoff, "Time-correlation function description of absorption lineshapes," 2009.

[40] K. Vandewal, K. Tvingstedt, A. Gadisa, O. Inganas, and J. Manca, "On the origin of the open-circuit voltage of polymer-fullerene solar cells," *Nature Materials*, vol. 8, pp. 904–909, Nov. 2009.

Auteursrechtelijke overeenkomst

Ik/wij verlenen het wereldwijde auteursrecht voor de ingediende eindverhandeling:
Spectroscopic methods for the study of artificial photosynthesis

Richting: **master in de biomedische wetenschappen-bio-elektronica en nanotechnologie**
Jaar: **2010**

in alle mogelijke mediaformaten, - bestaande en in de toekomst te ontwikkelen - , aan de Universiteit Hasselt.

Niet tegenstaand deze toekenning van het auteursrecht aan de Universiteit Hasselt
behoud ik als auteur het recht om de eindverhandeling, - in zijn geheel of gedeeltelijk -,
vrij te reproduceren, (her)publiceren of distribueren zonder de toelating te moeten
verkrijgen van de Universiteit Hasselt.

Ik bevestig dat de eindverhandeling mijn origineel werk is, en dat ik het recht heb om de rechten te verlenen die in deze overeenkomst worden beschreven. Ik verklaar tevens dat de eindverhandeling, naar mijn weten, het auteursrecht van anderen niet overtreedt.

Ik verklaar tevens dat ik voor het materiaal in de eindverhandeling dat beschermd wordt door het auteursrecht, de nodige toelatingen heb verkregen zodat ik deze ook aan de Universiteit Hasselt kan overdragen en dat dit duidelijk in de tekst en inhoud van de eindverhandeling werd genotificeerd.

Universiteit Hasselt zal mij als auteur(s) van de eindverhandeling identificeren en zal geen wijzigingen aanbrengen aan de eindverhandeling, uitgezonderd deze toegelaten door deze overeenkomst.

Voor akkoord,

Robaeys, Pieter

Datum: **16/06/2010**